THE INFLUENCE OF SONICATION DURING THE PURIFICATION OF THE VITAMIN D RECEPTOR PROTEIN

by

Tahniyath Ara Zaman

A Thesis Submitted in

Partial Fulfillment of the

Requirements of the Degree of

Master of Science

in Chemistry

at

The University of Wisconsin-Milwaukee

May 2012

THE INFLUENCE OF SONICATION DURING THE PURIFICATION OF THE VITAMIN D RECEPTOR PROTEIN

by

Tahniyath Ara Zaman

A Thesis Submitted in

Partial Fulfillment of the

Requirements of the Degree of

Master of Science

in Chemistry

at

The University of Wisconsin-Milwaukee

May 2012

Major Professor   Date

Graduate School Approval   Date

ABSTRACT

THE INFLUENCE OF SONICATION DURING THE PURIFICATION OF THE VITAMIN D RECEPTOR PROTEIN

by

Tahniyath Ara Zaman

The University of Wisconsin-Milwaukee, 2012
Under the Supervision of Dr. Alexander Arnold

The Vitamin D Receptor (VDR) is a ligand-dependent transcription factor that belongs to the nuclear receptor superfamily. Upon binding to its natural ligand 1 α, 25-dihydroxyvitamin D_3, VDR regulates many functions including cell growth and differentiation, bone mineral homeostasis, development, immune function and hair follicle cycle. During the purification of VDR protein, we observed that the time of sonication, to break the cell membrane, has a strong influence on the VDR functionality, as measured by the affinity for coregulator proteins. This investigation determines the dependency between sonication, temperature and functionality of VDR protein during purification. We have expressed recombinant human vitamin D receptor-ligand binding domain (VDR-LBD) fused with maltose binding protein (MBP) in *Escherichia coli* BL21 cells and purified the protein under different conditions using amylose affinity

chromatography. The ability of purified VDR-LBD to bind to the coregulator peptide SRC2-3 in the presence of the synthetic analog of vitamin D receptor LG190178 was determined by fluorescence polarization. The K_d values ranged between 30.7 nM and 368.2 nM. The purified protein fractions were also investigated for stability by differential scanning calorimetry.

_____

Major Professor   Date

AKNOWLEDGEMENTS

TABLE OF CONTENTS

LIST OF FIGURES

LIST OF TABLES

LIST OF ABBREVIATIONS

$(1\alpha, 25\ (OH)_2\ D_3)$,……………………………………..$1\alpha$,25-dihydroxyvitamin D_3

AF-2………………………………………...…….……….Activation function 2

BSA…………………………………………….……….Bovine serum albumin

(ΔC_p)……………………………………….…………Change in molar heat capacity

DBD……………………………………………….....DNA binding domain

DMSO…………………………………………………Dimethyl sulfoxide

DRIP…………………………………………….. VDR-interacting protein

DSC…………………………………..…….…..Differential Scanning Calorimetry

DTT………………………………………………….…Dithiothreitol

E.coli……………………………………………………...*Escherichia coli*

EDTA……………………………………….Ethylenediaminetetraacetic acid

FP………………………………………………….…Fluorescence polarization

(ΔG) ….………………………………………...Change in Gibbs free energy

(ΔH)………………………………………………….………..Change in enthalpy

HDAC………………………………………………...Histone deacetylases

IPTG………………………………...…Isopropyl 1-thio-β-D-galactopyranoside

K_d... Dissociation constant

LB…………………………………………...……Lysogeny Broth /Lauria-Bertani

LBD……………………………………………..………Ligand binding domain

MBP……………………………………………..……...Maltose binding protein

VDR-LBDmt………...……………..…Mutated vitamin D receptor-ligand binding domain

mVDR…………………………………………….……Membrane-bound receptor

1. Introduction

Vitamin D Receptor (VDR) is one of the 48 nuclear receptors present in humans. VDR is a ligand-activated transcription factor present in the cytosol and nucleus of cells. VDR plays an important role in many cellular and physiological processes by altering expression of genes responsible for bone mineral homeostasis, immune function, metabolism, hair follicle cycle, and cell proliferation and differentiation. VDR binds very strongly to the biologically active form of vitamin D, 1α, 25-dihydroxyvitamin D_3 (1α, 25 $(OH)_2D_3$) [1]. Upon binding to the ligand, VDR undergoes a conformational change to form activation function 2 (AF-2). The activation function 2 is a hydrophobic cleft formed by three helices and a short amphipathic α-helix (H12) at the carboxy terminus [2] and creates a binding surface for coactivators. Coactivators are proteins that interact with many nuclear receptors, such as VDR, to regulate transcription by facilitating the assembly of basal transcription machinery. These include the steroid receptor coactivators (SRCs) that interact with VDR [3] and have histone acetyltransferase activity [4]. Histone acetyltransferases (HATs) are a class of enzymes that play an important role in gene transcription by remodeling the chromatin structure [5]. HATs target histones that are bound to DNA and destabilize the nucleosomal core by catalyzing the acetylation of lysine residues present in the N-terminal tails of histones. This catalytic activity unwinds the DNA, which becomes a target for another coactivator known as VDR-interacting protein (DRIP) complex [6]. The coactivator DRIP contains additional proteins known as the mediator factors that are required for interaction with basal transcriptional machinery to initiate transcription[7]. Additionally, VDR interacts with transcriptional intermediate

factor 1α [TIF1α] and the suppressor of gal1 [SUG1] [8], which is involved in the modulation of the chromatin structure [9].

In the absence of the ligand, VDR is associated with corepressors such as the nuclear receptor corepressor (N-CoR) and the silencing mediator of retinoic acid and thyroid hormone receptor (SMRT)[10]. N-CoR and SMRT are corepressor proteins that function to repress the transcriptional activity of VDR. These corepressor proteins bind specifically to the hydrophobic cleft on the VDR-LBD. Binding of the corepressor proteins induces the recruitment of the histone deacetylases (HDAC) [11]. The histone deacetylases are a class of enzymes that play an important role in the regulation of gene expression by removing the acetyl groups that are present on the lysine residues on the histone N-terminal "tails". Consequently, deacetylation of the histone tails results in a more compact chromatin structure and prevents the RNA polymerase from initiating transcription.

Upon ligand binding, the corepressors are released from the VDR and the coactivators are recruited. Also, the VDR forms a heterodimer with retinoid X receptor (RXR) [12]. RXR is a nuclear receptor for 9-cis retinoic acid, and it is an obligate partner of VDR in mediating gene expression. In the presence of the natural ligand 1α, 25 $(OH)_2$ D_3, it induces RXR and VDR heterodimerization and translocation of the complex into the nucleus. The heterodimeric complex then binds to a specific sequence on the DNA known as the vitamin D response elements (VDRE) [13]. The VDREs are generally located in the promoter region of VDR target genes in order to regulate gene expression as shown in **figure-1.**
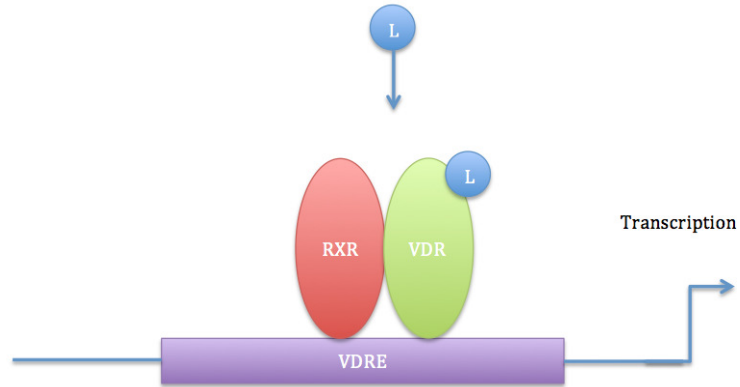
Figure 1 Ligand activated transcription. Ligand binding to the vitamin D receptor causes heterodimerization with retinoid X receptor. The heterodimeric complex binds to the vitamin D response elements on the DNA and activates transcription.

1.1 Vitamin D Receptor Structure

The human VDR is comprised of 427 amino acids and it contains several functional domains including four regions designated A-F in **figure-2**:
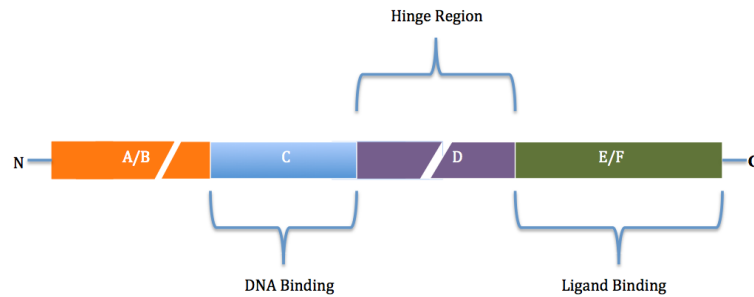
Figure 2 VDR domains. N-terminal domain (A/B), DNA-binding domain (C), hinge region (D), and C-terminal ligand binding domain (E/F).

Members of the superfamily of the nuclear receptors contain a similar modular structure with a variation in the N-terminus of the A/B domain. Among the nuclear receptors the A/B region is the most divergent domain and it contains an autonomous activation function, AF-1. However, VDR lacks the AF-1 and the A/B domain is relatively short compared to the other domains. The A/B domain is non-conserved and it comprises of all residues amino terminal to the DNA binding domain.

The C region also known as the DNA-binding domain (DBD) is a highly conserved region [14]. This domain consists of two similar modules, each containing a zinc finger motif. The zinc ions are coordinated in a tetrahedral fashion through four highly conserved cysteine residues that stabilize the finger structure. These two modules have two different functions in DNA binding. First, the amino-terminal module directs specific DNA binding in the major groove of the DNA binding site on the protein.

Second, the carboxy-terminal module serves as a dimerization interface for interactions with other proteins. The key feature of the zinc fingers is that they have α -helices at the carboxy-terminal, which is very important in the interaction with DNA.

The D domain is the hinge region, which is a highly flexible region of the vitamin D receptor. The hinge region is not a conserved region among VDRs from other species, or among other members of the nuclear receptor superfamily. The hinge region links the DBD and the LBD of VDR and allows the rotation of the DBD in order to reduce the steric hindrance between the DBD and LBD.

The E region is the ligand-binding domain (LBD) and it is a moderately conserved domain among the nuclear receptors. The LBD is one of the most important domains, responsible for ligand binding, dimerization, and coregulator interactions. The LBD consists of 12 α-helices (H1-H12) arranged in an anti-parallel α-helical sandwich. The vitamin D receptor LBD also contains three β sheets [15]. Once VDR binds it's natural ligand 1,25-dihydroxyvitamin D_3 it can accommodate coactivators as depicted in the crystal structure that shows liganded VDR bond to the coactivator peptide DRIP2 in **figure-3**.
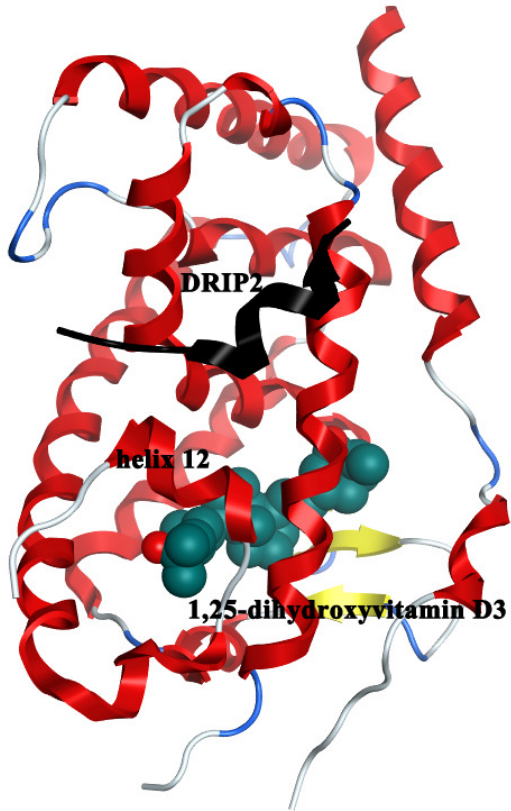
Figure 3 Crystal structure of the human VDR-LBD, bound to the ligand 1α, 25-dihydroxy vitamin D3 and coactivator peptide DRIP2 2.

1.2 Biosynthesis of Vitamin D3

The active metabolite of vitamin D_3 is 1α, 25-dihydroxyvitamin D_3 (1α, 25 $(OH)_2$ D_3), which is a metabolic product as shown in **figure-4**. Vitamin D_3 can either be obtained from the diet or it can be synthesized from the fat soluble pro-hormone 7-dehydrocholesterol via a non-enzymatic, ultraviolet light-dependent reaction [16].
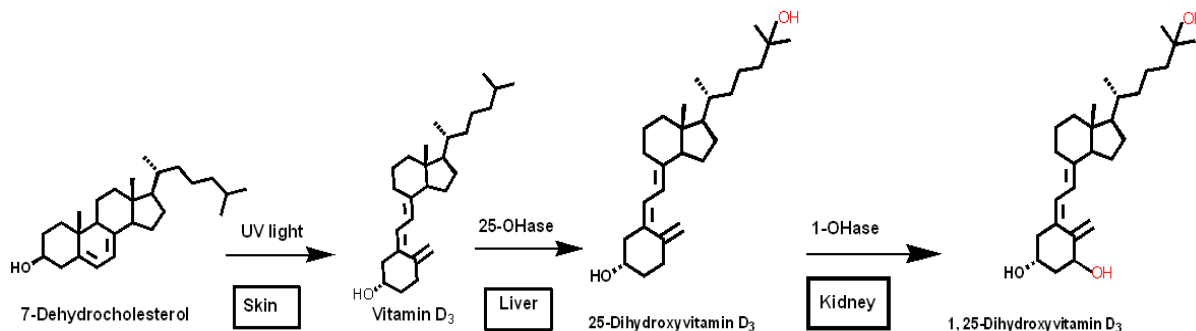
Figure 4 1α, 25-Dihydroxyvitamin D3 (Calcitriol) Formation.

Vitamin D_3 has two main activation steps. In the first activation step, vitamin D_3 enters the liver through the blood circulation and it is hydroxylated at the 25th position of the side chain to produce 25-hydroxyvitamin D_3 by the enzyme 25-hydroxylase [17]. The second activation step occurs in the kidney. In this step, 25-hydroxyvitamin D_3 gets converted to 1α, 25 dihydroxyvitamin D_3 by the enzyme, 25-hydroxyvitamin D_3- 1-α – hydroxylase as shown in **figure-5** [18]. The activated hormone 1α, 25 dihydroxyvitamin D_3 then binds to its chaperone, the vitamin D binding protein, [19] and is shuttled through the body reaching virtually all cells. Additionally, the inactive precursor 25 dihydroxyvitamin D_3 is distributed the same way. Being a fat soluble molecule, 1α, 25 dihydroxyvitamin D_3 can enter the cell and activates its receptor (VDR) in the cytosol, which triggers the redistribution of the liganded VDR into the nucleus. Upon binding to 1α, 25-$(OH)_2$ D_3 VDR becomes activated, and then forms a complex with 9-cis-retinoic acid receptor (RXR) as shown in **figure-5**. The activated VDR-RXR complex then binds to the VDR response elements (VDREs), which are located in the promoter region of the gene. Binding to VDREs recruits other nuclear proteins known as the co-activators. The

resulting complex is then associated with RNA polymerase II (RNA Pol II) to initiate gene transcription[20],[21],[22].
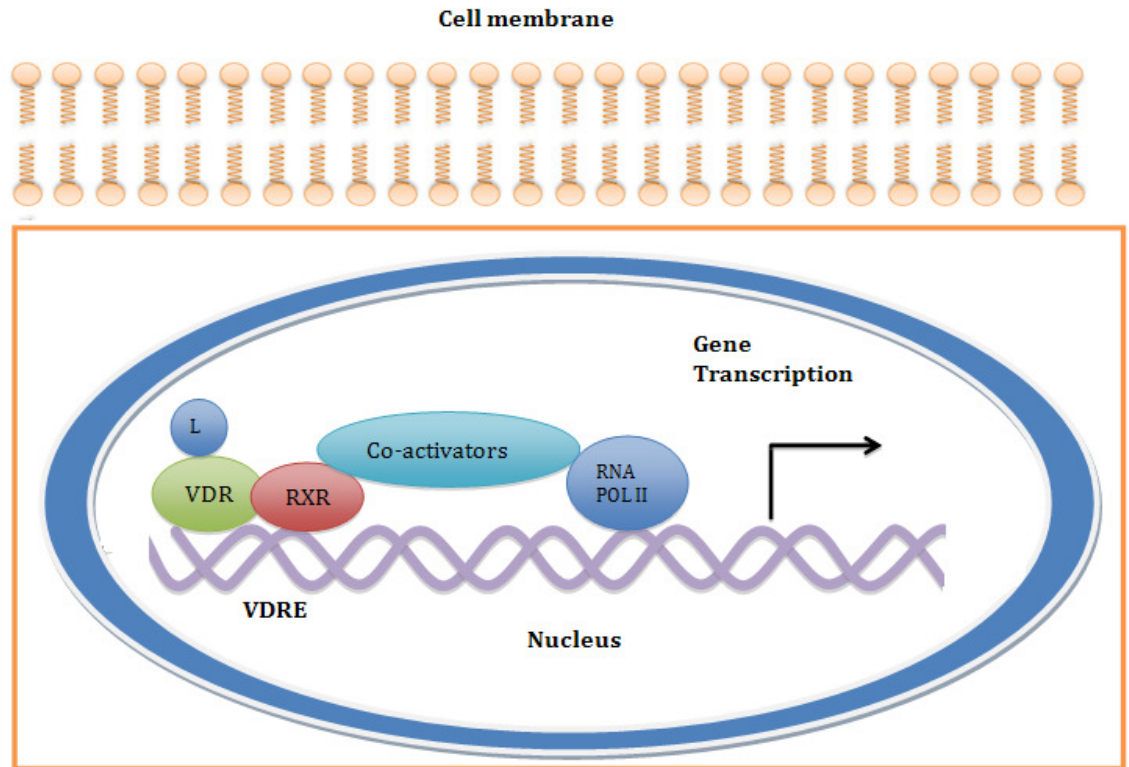
Figure 5 Ligand activated gene transcription.

1.3 Previous work

VDR was first cloned in 1987 [23] and the first crystal structure of a VDR-LBD mutant was determined by Rochel et al in 2000[15]. Although many researchers identified the interactions of VDR-LBD with coactivators and corepessors, it was not until 2009 that the binding constants between VDR-LBDmt and different nuclear interaction domains of several coregulators were quantified [24]. At that point the mutant VDR-LBD containing the residues 118-425 and lacking the residues Δ165-215 was cloned into the pMal-c2x vector, and expressed in *E. Coli*, and purified. The binding constants between VDR and fluorescently labeled coregulator peptides were determined in the presence of the synthetic non-secosteroid agonist LG190178 and calcitriol using fluorescence polarization. The third nuclear interaction domain of the steroid receptor coactivator 2 (SRC2-3) showed the highest binding affinity among the SRCs tested, with a K_d value of 840nM. However, VDR-LBD protein batches prepared on different days resulted in a relatively broad K_d value range of ± 300 nM.

1.4 Hypothesis

The goal of this project was to identify protein expression and purification conditions for the VDR-LBDmt to produce protein that results in the highest binding affinity (lowest K_d) towards coregulator peptide SRC2-3. During the purification process we found that the time of sonication, to break the bacterial cell membrane, had a strong influence on the functionality (binding toward coregulator peptide SRC2-3) of VDR-LBDmt. Physically, the time of sonication influences the temperature of the cell lysate,

which in turn influences the folding of protein and therefore affects the ability of VDR-LBD to recruit the coactivator peptide SRC2-3.

In this thesis, we describe the relationship between sonication time, temperature of the cell lysate, protein stability, and functionality of VDR-LBD. Therefore, we are using fluorescence polarization to access the binding affinity and a thermofluor stability assay and differential scanning calorimetry for determining protein stability.

2. VDR-LBD Expression and Purification

2.1 Description of the VDR-LBDmt plasmid

VDR-LBDmt was expressed in the *E. coli* as a maltose binding protein (MBP) fusion. There are many advantages of using the maltose binding protein. It prevents the formation of inclusion bodies during protein production, which can form insoluble and biologically inactive aggregates[25]. Also, the MBP helps to enhance the solubility of its fusion partner, in our case VDR-LBD. The exact mechanism of how MBP helps to enhance the solubility of its fusion partner is unknown, but it is hypothesized that it acts as a chaperone and prevents self-association of its fusion partner. Another advantage of using the MBP is that this protein is known to be the only general solubilizing agent which can also be used as an affinity tag [25].
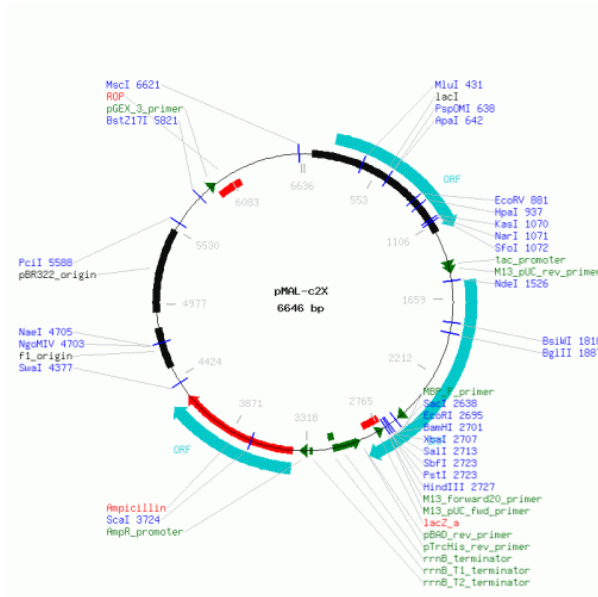
Figure 6 Vector map of pMAL-c2X (New England Biolabs).

The vector pMAL-c2X (purchased from New England Biolabs) was used to produce the fusion protein maltose-binding protein fused with mutated vitamin D receptor-ligand binding domain (MBP-VDR-LBDmt). The plasmid vector contains three important sites indicated by the red areas (**figure-6**). The first of these is the cloning site or open reading frame, where the DNA fragment of VDR-LBDmt was inserted into the restriction site of the vector polylinker. A *mal*E-*lac*Za combination of restriction enzymes was used for the insertion. The plasmid vector also contains a drug resistance gene for ampicillin, which allows selective growth of host *E.coli* cells carrying plasmid. Finally, the pMAL-c2X vector also contains a replication origin to allow the plasmid to be replicated in the host cell.

The VDR-LBDmt gene provided by D. Moras was amplified with the polymerase chain reaction, using the primers 5′-CGCGGATCCAGATCTGACAGTCTGCGGCCCAAG- 3′ and 5′-

11

CGCGGATCCAGATCTGACAGTCTGCGGCCCAAG-3′. The gene of VDR-LBDmt contains residues 118-425 and lacks the sequence Δ165-215. This fragment was inserted downstream from the malE gene, which encodes for maltose binding protein resulting in the expression vector for MBP-VDR-LBDmt [24]. The recombinant plasmid was then inserted into competent *E.coli* cells via transformation.

2.2. Plasmid Transformation

A tube of the BL21 competent *E. coli* cells (purchased from New England Bio Labs) were removed from the -80 ^{0}C and thawed on ice for 10 minutes. 1 μL of the recombinant plasmid DNA containing MBP-VDR-LBDmt was added to the cell mixture in the tube. The tube was carefully flicked 4-5 times to mix the DNA and the cells. The DNA-cell mixture was placed on ice for 30 minutes, then placed in a warm water bath at 42^{0}C for exactly 10 seconds for heat shock to take up the plasmid into the *E.coli* cells. The mixture was placed on ice for 5 minutes to close the pores of the cells. 950 μL of super optimal broth (SOC), a nutritional medium for bacterial growth of *E.coli,* was added to the DNA-cell mixture and incubated at 37^{0}C for 1 hour with vigorous shaking. After one hour, 50μL of the mixture was plated onto a Lauria-Bertani (LB) agar plate containing 100mg/L carbenicillin and incubated overnight at 37^{0}C.

2.3 VDR-LBDmt Protein Expression

The next day, a single colony was abstracted from the agar plate and added to a flask containing 500 ml of Luria-Bertani (LB) broth (termed seed culture, used 1 pre-weighted LB capsule) and 100 mg/L carbenicillin (antibiotics), and incubated overnight

at 25 ^{0}C with vigorous shaking. The LB broth was purchased from Research Products International Corp as premeasured and premixed capsules. For the final solution, a 20 gram capsule was used containing the following contents; 10g Tryptone, 5g NaCl, 5g yeast extract, and 1.5g Tris/Tris HCl [26]. Two capsules were added to 1L of H_2O and sterilized by autoclaving. To the cooled (room temperature) media 1 ml of carbenicillin stock solution (1000x) was added. The stock solution of carbenicillin was prepared by dissolving 1 g of carbenicillin in 10 ml Millipore H_2O. The next day, 25 ml of the seed culture were added to each of the prepared 1L LB media flasks with 100mg/L carbenicillin and the culture was stirred vigorously at 25 ^{0}C until the OD_{600} reached 0.6.

A stock solution of 0.2 mM Isopropyl 1-thio-β-D-galactopyranoside (IPTG) was first prepared by dissolving 238.3 mg in 50 ml of MilliQ H_2O. From the stock solution, 1 ml of IPTG was added to each flask containing 1L of LB media and carbenicillin and incubation was continued on the shaker/incubator set at 250 rpm for 16 hours at 25^{0}C. The next day, cells were harvested by centrifugation at the speed of 4000 rpm at 4^{0}C and the bacteria pellet was transferred into 50 ml conical tubes. Each conical tube contained a cell pellet that was harvested from 2 liters of the LB media after centrifugation. The cells were then stored in the -80^{0}C freezer to be used later for purification.

2.4 VDR protein purification

In order to purify MBP-VDR-LBDmt, the cells from protein expression were removed from the -80^{0}C freezer and thawed in cold tap water for several minutes, until the frozen cell pellet became soft and smooth. The resulting pellet was re-suspended in the column buffer containing 20 mM Tris-Base (pH 7.5), 0.5 mM EDTA, 1 mM Sodium

azide, 200 mM NaCl, 1 mM DTT, with EDTA-free protease inhibitor cocktail (Roche Diagnostics) [26]. The protease inhibitors inhibit the proteolytic activity by the enzymes known as proteases present in the *E. coli* bacteria. The proteases cleave the peptide bonds that link the amino acids together to form proteins. The proteases inhibited by this cocktail of inhibitors are serine proteases, threonine proteases, cystein proteases, aspartate proteases, glutamic acid proteases and metalloproteases.

Sonication is one of the most popular techniques used for lysing small quantities of *E. coli* cells. Sonication uses the ultrasound waves to agitate particles in the sample to break the cell membrane. The main problem with sonication is controlling the temperature of the cell suspension while sonicating. Therefore, we used an ice bath or ice/salt mixture for cooling.

For cell lysis, the 50 ml conical tubes containing the re-suspended cell pellet were placed in the ice bath and sonicated. Sonication was applied with short pulses of 5 seconds separated by 5 seconds rest, and the amplitude was set at 40%. Sonication was performed for varying times and the temperature was recorded before and after sonication. Four different 50 ml conical tubes were sonicated with variable times in three cycles. For the different conditions we labeled the VDR protein as 1, 2, 3, 4. The recorded temperatures before and after sonication for each cycle and the sonication times are shown in **table-1**. For protein 1 we used a salt/ice mixture to maintain the low temperature.

Table 1 Summary of temperatures found for different sonication times.

	Number of cycles	Initial and final temperature recorded	Sonication time
*Protein-1 Ice/salt mix	1	$4\text{-}5^0\text{C}$	30 secs
	2	$4\text{-}7^0\text{C}$	30 secs
	3	$4\text{-}8^0\text{C}$	30 secs
Protein-2	1	$4\text{-}10^0\text{C}$	42 secs
	2	$4\text{-}10^0\text{C}$	42 secs
	3	$4\text{-}9.5^0\text{C}$	42 secs
Protein-3	1	$4\text{-}18^0\text{C}$	2 mins
	2	$4\text{-}15^0\text{C}$	1 min and 30 secs
	3	$4\text{-}15.5^0\text{C}$	1 min and 30 secs
Protein-4	1	$4\text{-}18^0\text{C}$	2 mins
	2	$4\text{-}18^0\text{C}$	2 mins
	3	$4\text{-}22^0\text{C}$	2 mins and 30 secs

The temperatures were recorded for three different cycles with increasing time of sonication. Sonication provides high frequency of sound waves to agitate and lyse cells. The agitation of the probe can cause excessive heating of the sample, and may degrade the protein that is present inside the bacterial cell membrane. Therefore the sample was immersed in an ice bath for cooling, and to prevent the degradation of protein.

After sonication, the debris from the cell lysate was removed by centrifugation at 18,000 rpm for 45 minutes at 4°C. The supernatant containing VDR-LBD was used for purification.

The amylose resin (purchased from New England Bio Labs) was prepared by washing with column buffer containing 20 mM Tris-Base (pH 7.5), 0.5 mM EDTA, 1 mM Sodium azide, 200 mM NaCl, 1 mM DTT.The fusion protein consists of the VDR-

LBD fused with maltose binding protein (MBP). Generally, the MBP binds to maltose, but it can also bind to amylose [27]. The amylose resin was washed with column buffer 3 times prior to use. About 5 ml of amylose resin was added to each of the 50ml conical tubes containing the cleared lysate, and the suspension was mixed by oscillating inversion overnight at 4^0C on the rotator, to ensure binding between MBP and solid supported amylose.

The resulting suspension was centrifuged at 4000 rpm for 20 minutes at 4^0C. The pellet was collected for purification referred to as Batch-1. The supernatant was collected and incubated overnight with 5 ml amylose resin as before. The resulting VDR-LBD protein from the second incubation is described later as Batch-2.

The resin containing the VDR-LBD protein was washed 5-7 times with column buffer. The supernatant was discarded after each wash. The protein was eluted with column buffer in 5-7 fractions containing 10 mM maltose. The eluted fractions were pooled and spun for 4 minutes at 4000rpm at 4^0C followed by dialysis in order to concentrate the diluted fractions and to reduce the volume.

The pooled protein was dialyzed overnight using a 10,000 MW dialysis cassette (purchased from Pierce). The dialysis cassettes were placed in dialysis buffer at 4^0 C overnight containing 20 mM Tris-base (pH 7.4), 100 mM NaCl, 1 mM EDTA, 1mM Sodium Azide, 1 mM Dithiothreitol (DTT), 10% Glycerol, and 0.01% NP-40. A concentrated 40X solution was pre-made without glycerol and NP-40 detergent, and it was diluted in millipore water to 3.5 L, followed by the addition of 400 ml glycerol 400 µl NP-40. The VDR protein was dialyzed over night. The next day, the dialysis cassette

was transferred into a 4L of fresh dialysis buffer for 6 hours. Concentration of the

purified protein was carried out using the Corning Spin-X UF, 10,000MW concentrators.

2.5 Determination of VDR-LBD Concentrations Using the Bradford Assay

The Bradford Assay was performed to determine the concentration of VDR-LBD

protein. In this assay an acidic reagent known as the Coomassie Brilliant Blue G-250 dye

(purchased from Pierce) was used. The Coomassie blue reagent contains the acidic

environment in which the protein binds to the Coomassie dye. The protein-dye complex

causes a spectral shift from 465 nm to 595 nm, changing the color from brown to the blue

form of the dye. Therefore, the wavelength of 595 nm is the optimal wavelength to

measure the absorbance of the protein-dye complex[28], [29].

In order to obtain the concentration of the purified protein, six standard solutions

were prepared using bovine serum albumin (BSA). The standard solutions in water

contained 0.625, 1, 2, 3, 4, and 5 mg/ml of BSA, respectively. In a 96 well optical clear

plate, 200 µL of the Coomassie Brilliant Blue G-250 was mixed with 1 µL of the BSA

standard solutions in duplicate. The well plate was incubated at room temperature with

vigorous shaking for 30 seconds. The absorbance was recorded at 595 nm using a Tecan

microplate reader (M1000). A standard curve was plotted using Microsoft Excel with

concentration of BSA in mg/ml on the x-axis and absorbance at 595 nm on the y-axis.

Then, the straight-line equation Y=mx+b was computed as depicted in **figure-7**.
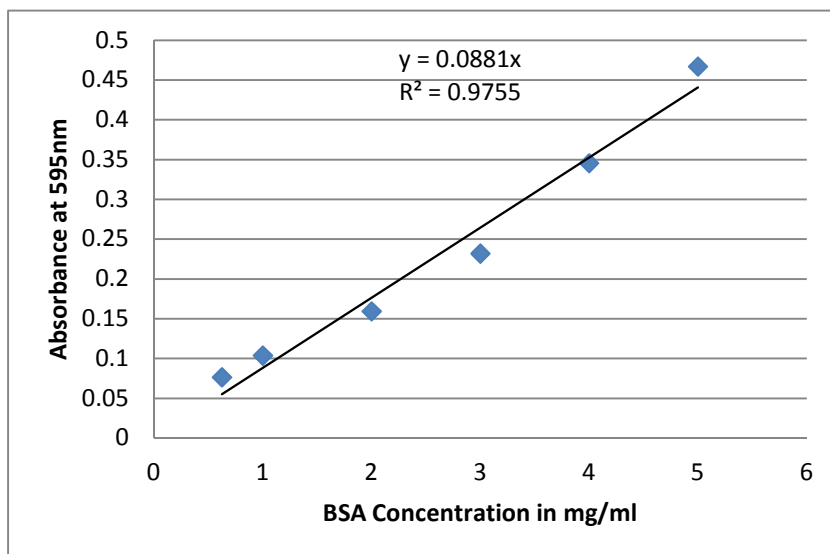
Figure 7 Standard Bradford Assay Graph using the Bovine Serum Albumin (BSA) protein. A linear graph for plotted using the increasing concentration of BSA and the absorbance was measure at the wavelength of 595 nm. The slope of the line was used to calculate the concentration of the MBP-VDR-LBDmt protein.

The concentrations of the different batches of purified MBP-VDR-LBD protein were determined using the slope of the equation[26] shown in **figure-7** and the results are summarized in **table-2.**

Table 2 Summary of different concentrations and yields of VDR-LBD protein.

Protein-1 (4-5^{0}C)	Batch	Date of purifi-cation	Amount in mg	Average amount (mg)	SD (mg)	Concen-tration (mg/ml)[1]	Concen-tration (µM)[2]
1	Batch-1	4/4/2011	8.95			4.26	56.82
2	Batch-1	4/21/2011	12.75	8.63	3.21	3.75	50.02
3	Batch-1	5/20/2011	7.84			8.71	116.17
4	Batch-1	7/14/2011	4.99			12.47	166.24
5	Batch-2	4/4/2011	6.71			3.53	47.12
6	Batch-2	4/21/2011	4.77	6.05	0.94	2.81	37.43
7	Batch-2	5/20/2011	5.92			3.12	41.54
8	Batch-2	7/14/2011	6.83			6.21	82.83
Protein-2 (4-10^{0}C)							
9	Batch-1	4/4/2011	8.58			4.51	60.18
10	Batch-1	4/21/2011	11.45	8.06	2.88	4.24	56.55
11	Batch-1	5/20/2011	4.43			11.07	147.54
12	Batch-1	7/14/2011	7.79			11.12	148.32
13	Batch-2	4/4/2011	4.05			1.76	23.49
14	Batch-2	4/21/2011	4.88	4.31	1.08	1.95	26.02
15	Batch-2	5/20/2011	5.40			3.38	45.03
16	Batch-2	7/14/2011	2.92			4.87	64.93
Protein-3 (4-15^{0}C)							
17	Batch-1	5/20/2011	15.81	9.78	8.52	12.16	162.11
18	Batch-1	7/14/2011	3.76			12.53	167.08
19	Batch-2	5/20/2011	8.35	9.18	1.17	6.42	85.65
20	Batch-2	7/14/2011	10.01			12.52	166.89
Protein-4 (4-20^{0}C)							
21	Batch-1	5/20/2011	11.85	7.91	5.56	11.85	158.06
22	Batch-1	7/14/2011	3.98			13.26	176.74
23	Batch-2	5/20/2011	4.94	7.85	4.11	2.35	31.35
24	Batch-2	7/14/2011	10.76			8.27	110.32

[1]The BSA slope shown in **figure-7** was used to calculate the concentrations in mg/ml;
[2]data was converted to µM by using the molecular weight of 75,000g/mol for the MBP-VDR-LBDmt protein.

The concentrations of purified VDR-LBD ranged between 1.76 and 13.26 mg/ml.

The data in mg/ml were converted to µM by using the molecular weight of 75,000g/mol

for the MBP-VDR-LBD protein complex, which resulted in concentration ranging between 23.49 and 176.74 µM. The corresponding amounts of VDR-LBD protein for each 2 liter culture of transformed *E. Coli* ranged between 2.92 mg and 15.81 mg. This variation is very high but reflects the difficulties to standardize protein production in order to achieve constant yields. Additionally, we observed a trend of protein-1 and protein-2 with a higher yield for batch-1 in comparison with batch-2. This trend was not observed for protein-3 and protein-4; but may be due to the limited numbers of repetitions.

2.6 Determination of VDR-LBD Protein Purity via SDS-PAGE

In order to determine the purity of the MBP-VDR-LBD protein, sodium dodecyl sulfate-polyacrylamide gel electrophoresis (SDS-PAGE) was used [26, 30]. The dialyzed protein samples were separated on the 1.0 mm x 15 well 4-12% Bis-Tris Gels (purchased from Life Technologies, NuPAGE).

The protein solution was mixed with LDS sample buffer (4X) (purchased from Invitrogen) containing sodium dodecyl sulfate (SDS). SDS is an anionic detergent and it coats the protein with negative charge so when an electric field is applied, the protein migrates solely as a function of their molecular weights [30].

The sample was then heated for 10-15 minutes on a water bath at $85\text{-}90^0$C to ensure the denaturing of the protein. The sample was centrifuged for 1 minute to collect any vapors that collected on the lid of the tube from heating [30]. A protein ladder (See Blue Plus 2 Pre-stained standard purchased from Invitrogen) and the protein sample were

loaded onto the gel and the SDS gel was set to run at 200V for 45 minutes at room temperature.

After removing the gel from the holder, the gel was stained with Coomassie Brilliant Blue R-250 dye (purchased from Invitrogen) for 1 hour with gentle shaking. The Coomassie Brilliant Blue R-250 dye stains both the gel and the protein. The gel was de-stained with Millipore H_2O overnight with gentle shaking resulting in a clear background and visible protein bands. The gel was then photographed the next day.
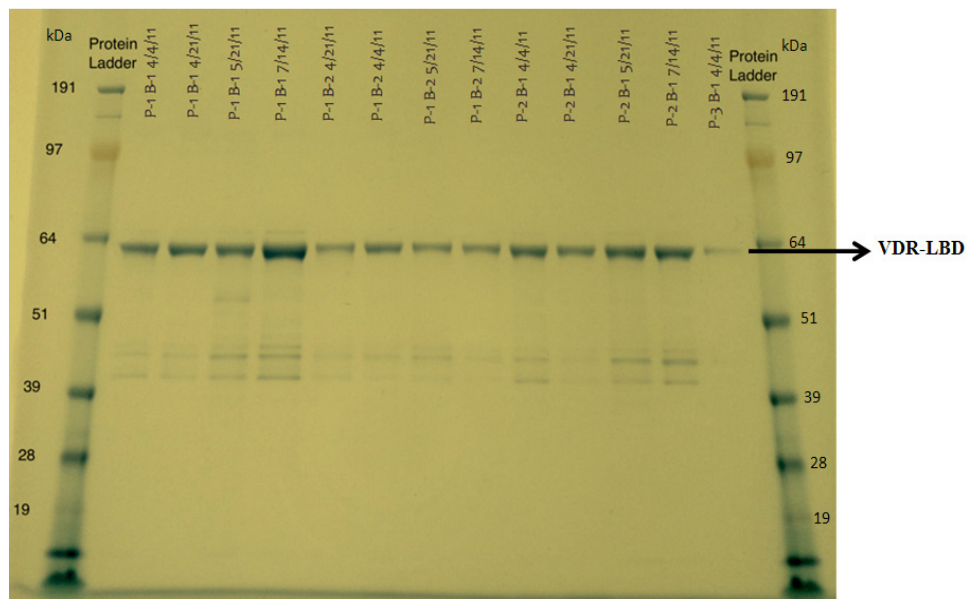
Figure 8 Coomassie-stained SDS-PAGE of VDR-LBD-MBP purified protein fractions. The molecular mass markers are indicated on the left and right side of the gel referred to as the protein ladder in kDa. Lanes 1-13 (active protein fractions) are labeled with the name and the date of purification. All lanes show a prominent band between 62-63kDa molecular weight, indicative of the VDR-LBD-MBP protein complex.
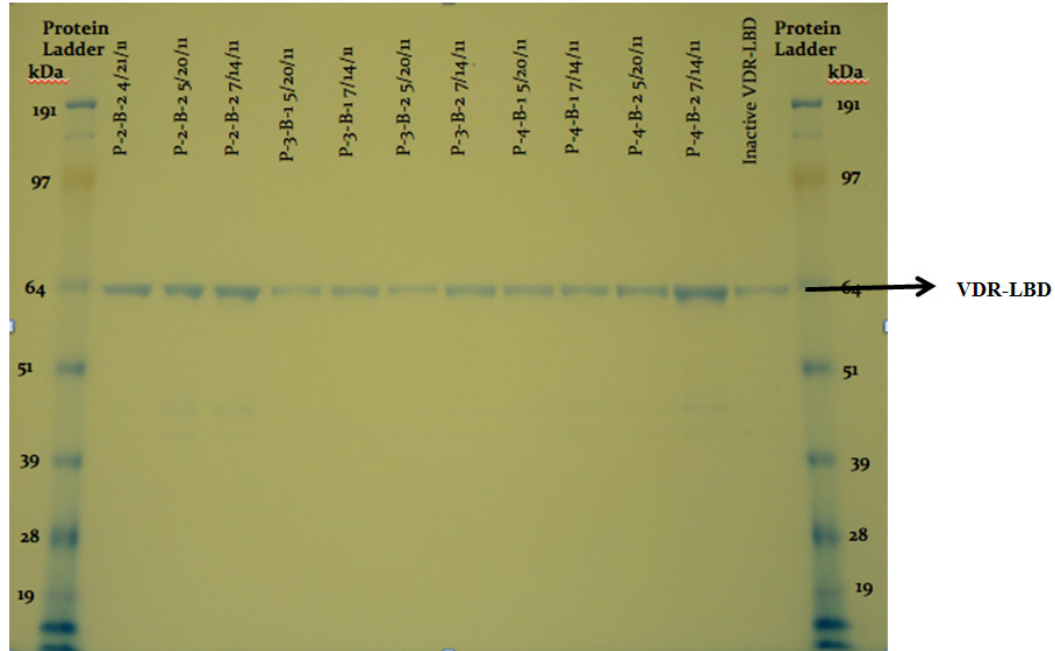
Figure 9 Coomassie-stained SDS-PAGE of VDR-LBD-MBP purified protein fractions, including the inactive protein. The molecular mass markers are indicated on the left and right side of the gel referred to as the protein ladder in kDa. Lanes 1-11 (active) are labeled with the name and the date of purification. Lane 12 is the Inactive VDR-LBD protein fraction. All the lanes show a prominent band between 62-63kDa molecular weight, indicative of the VDR-LBD-MBP protein complex present including the inactive VDR protein provided by Dr. Arnold.

All protein fractions show one predominant band near 64 kDa, which corresponds to VDR-LBD-MBP. The protein concentrations used for **figure 8** were higher than for **figure 9**, which resulted in faint but visible protein bands with smaller molecular weight. These bands may represent MBP generated by the empty MBP plasmid. In general the purity of all fractions is higher than 90% by visual inspection.

2.7 Discussion

We have developed a system for the production of recombinant human VDR-LBD in *E. coli* cells. Recombinant human VDR has previously been expressed in insect cells, yeast and *E. coli* [31]. One problem with expression in *E.coli* was the accumulation of VDR as insoluble inclusion bodies VDR. Therefore, an affinity tag of MBP was used not only to prevent the formation of inclusion bodies, but also to improve the yield and purity of VDR during purification. To study the quality and purity the protein samples were separated by SDS-PAGE, and all 24 protein fractions exhibited a band between 62-63kDa including the inactive protein (provided by Dr. Arnold) and the purity was above 90%.

3. Determination of the Functionality of VDR-LBD using Fluorescence Polarization Employing Coactivator Peptide SRC2-3

3.1 Introduction: Fluorescence Polarization

Fluorescence polarization (FP) was used to analyze the binding affinities of the MBP-VDR-LBD protein towards a fluorescent coactivator peptide SRC2-3. Fluorescence polarization is a powerful technique for studying molecular interactions including protein-protein, ligand-receptor, protein-DNA etc [32],[33].

Fluorescence polarization measures the changes in the orientation of plane polarized light brought about by fluorophores that undergo rapid molecular motion during their fluorescence lifetime. The lifetime of fluorescence is the period of time between absorption of an excitation photon and the emission of a photon through fluorescence [32],[33].
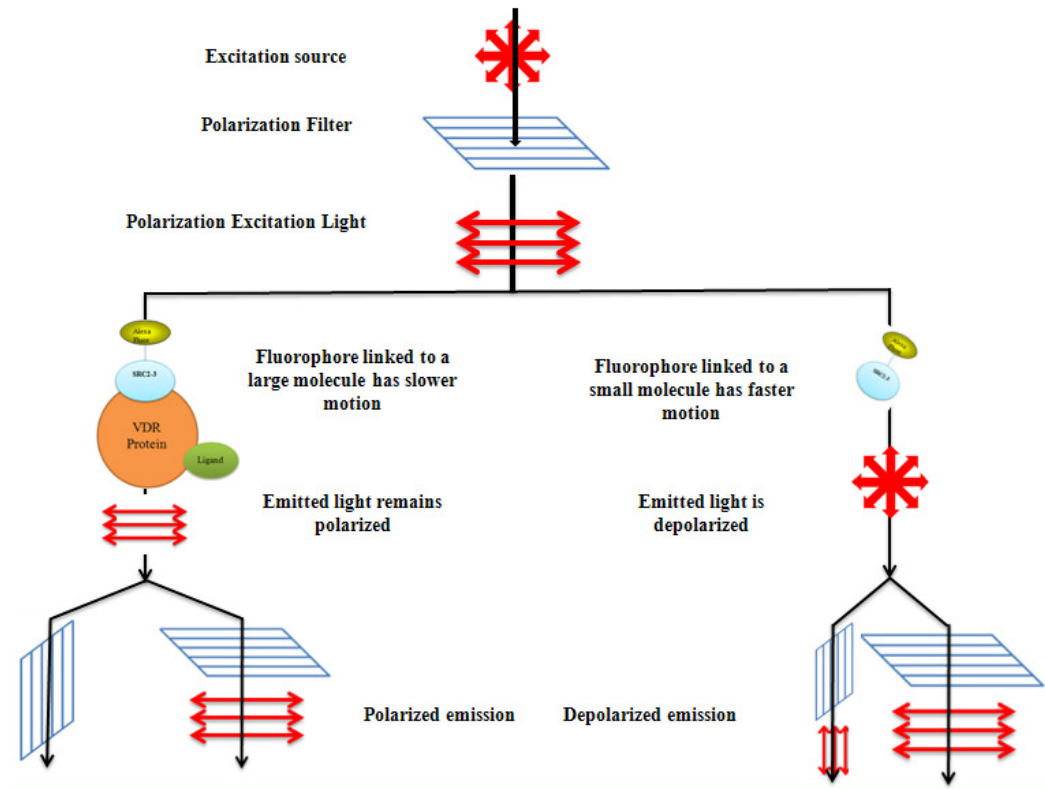
Figure 10 Fluorescence Polarization Assay. Unpolarized excited light is passed through a parallel polarization filter. The parallel polarized excitation light is absorbed by a big molecule attached to a fluorophore and remains polarized and enters another parallel and perpendicular polarized emission filter, and a high FP signal is detected. A small molecule attached to a fluorophore also absorbs light but the emitted light is depolarized then enters the parallel and perpendicular emission filters and a low FP signal is detected.

Polarization is the degree of uniformity of direction of the perpendicular transverse oscillation of a collection of light waves relative to their direction of travel [34].

$$P = \frac{Ivv - Ivh}{Ivv + Ivh}$$

P=Polarization

Ivv = Emission intensity of the vertically polarized light parallel to the plane of excitation

Ivh =Emission intensity of the horizontally polarized light perpendicular to the plane of excitation.

In order to measure the fluorescence polarization, there is loss of intensity at various points along the optical path. The incident light first passes through a monochronomator to select the incident wavelength. The incident light then passes through the vertical polarizer, shown in **figure-10**. Since only the vertical incident light passes through the polarizer, therefore, there is again a tremendous loss of intensity through this process. Then, the vertical polarized light passes through the sample in which only those fluorophores that are properly aligned absorbance dipoles will absorb the vertically polarized light. In this process only a small population of fluorophores will absorb the light and fluoresce, again the total outgoing light intensity will be decreased. The emitted light from the sample passes through another polarizer which is usually another monochromator in which the polarizer switches between the vertical and horizontal plane to detect the parallel and perpendicular intensity of emission.

Before measurement of sample polarization, the G-Factor was determined. This parameter corrects for instrumental polarization artifacts. The G-factor is determined with the following equation.

$$GF = \frac{Ihv}{Ihh}$$

Ihv =Intensity with excitation polarizer in the horizontal position and the emission polarizer in the vertical position

Ihh = Intensity with both excitation and emission polarizers in the horizontal position

The G-factor is the tendency of the grating to produce partially polarized transmitted light. The grating component of the G-factor is normally less than 1 [35]. The G-factor can strongly be wavelength dependent, but polarization is normally formed at fixed wavelength the polarization is corrected with the following equation[34].

$$P = \frac{Ivv - (GF\ X\ Ivh)}{Ivv + (GF\ X\ Ivh)}$$

In this study the fluorescence was measured in millipolization (mP) therefore

mP=1000X

3.2 The application of Fluorescence Polarization to Detect Protein-Protein Interaction

The fluorescently labeled peptide SRC2-3 molecule free in solution is excited with plane-polarized light at a wavelength of 635 nm and 685 nm for excitation and emission, respectively. Due to it's small molecular weight, the molecule tumbles rapidly in the solution causing the emission of depolarized light thus a low amount of polarized light can be detected after applying a parallel and perpendicular filter. When the MBP-VDR-LBD protein binds to the ligand LG190178, the ligand-receptor complex can recruit the fluorescently labeled peptide SRC2-3. Consequently, the molecular weight of

the resulting complex is increased significantly, and therefore the complex tumbles more slowly. It causes more emitted light to remain polarized in the same plane as the excitation plane. Therefore a high polarization signal is detected after applying a parallel and perpendicular filter allowing the detection of a ligand-binding to a larger macromolecule shown as in **figure-11** [36].
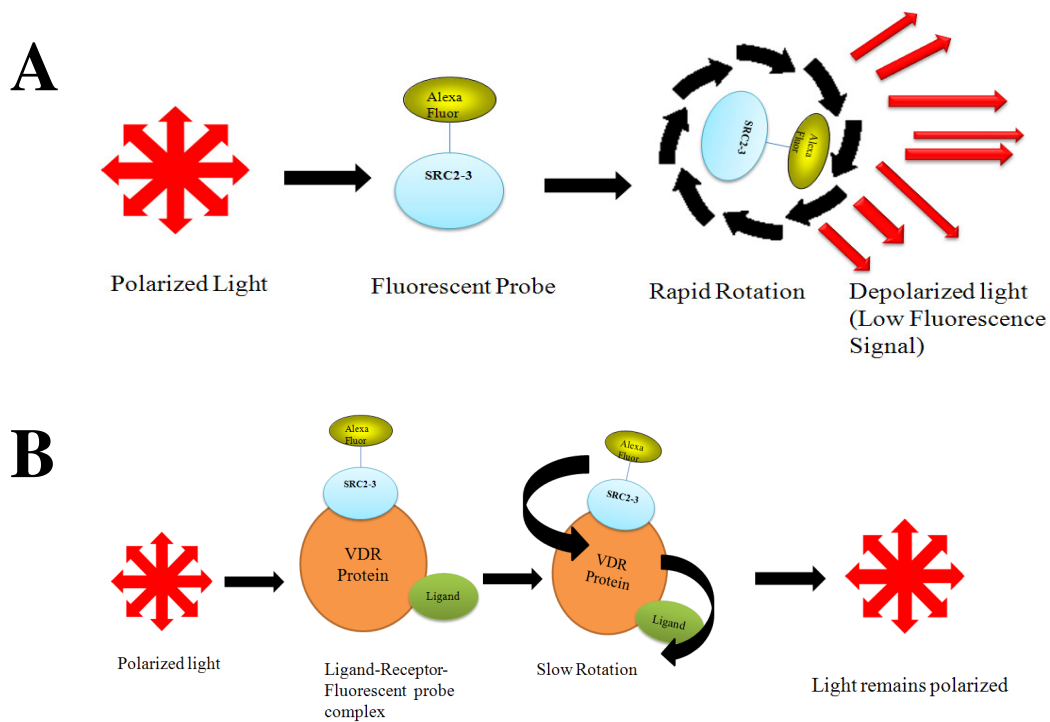
Figure 11 Protein-Protein Interaction using the Fluorescence Polarization Assay. A-Low FP signal due to the higher degree of depolarization. B-High FP signal based on low degree of depolarization.

3.2 Protocol to determine the interaction between VDR and coregulator SRC2-3

A fluorescence polarization binding assay was performed to measure the ability of different batches of the purified VDR-LBD to bind to its coactivator SRC2. A coregulator peptide steroid receptor coactivator (SRC2-3) was fluorescently labeled with Alexa Fluor 647 and used in the presence of a synthetic analog of vitamin D referred to as LG190178 [37], which was identified by Ligand Pharmaceuticals[22] . The structure is shown in **figure-12** [38]. Two different protein batches were tested separately, each carried out in quadruplets.
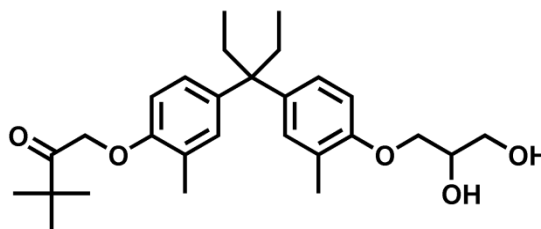
Figure 12 LG190178: Synthetic Agonist for Vitamin D Receptor.

In a 96 well plate round bottom (Corning Cat # 3365) MBP-VDR-LBD protein was serial diluted to 1:2 for 1-4 points then 1:5 for points 5-12 in the FP buffer containing 25 mM PIPES, 50 mM NaCl, 0.01% NP-40, 2% DMSO, (pH 6.75). Then 10 µL of the resulting solution was added to a 384 well plate (Corning) in quadruplets. 1 µL of the SRC2-3 labeled with Alexa Fluor 647 was diluted in 30 ml of the FP buffer. Of this solution 1.5 ml was combined with 1.8 µL of LG190178 ligand (from a stock solution of 10 mM stored in DMSO and mixed). The final concentration was 5 µM. 10 µL of this

solution was added to 10 μL of serial diluted VDR-LBD protein in a 384-well plate

resulting in a final volume of 20 μL in each well. The 384-well plate was centrifuged at

1000 rpm for 2 minutes at 4^0C to ensure a constant liquid level of all wells. A Tecan

Reader instrument (M1000) was used to measure the fluorescence polarization. The data

were fit to a sigmoidal dose-response curve using the Graph-Pad Prism software to obtain

the K_d values [24].

3.3 Results of Fluorescence Polarization assay

Twenty four different samples were evaluated by fluorescence polarization to test

the functionality and to determine the best purification conditions. Two examples are

depicted in **figure-13** and **figure-14**.
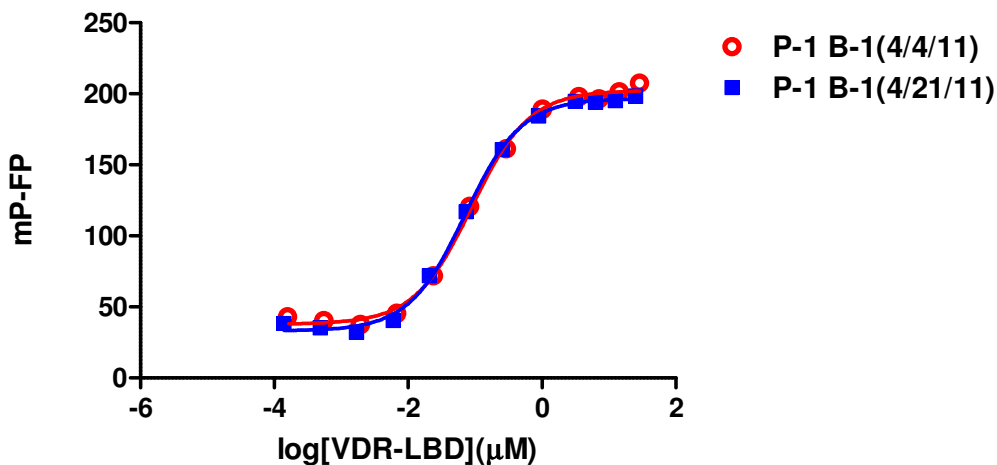
**Figure 13 Fluorescence polarization graph for VDR-LBD Protein-1 Batch-1 purified
on two different days**. The sigmoidal dose-response curve suggests that the VDR-LBD
protein is active. The fluorescence polarization assay was performed by maintaining a
constant concentration of the fluorescently labeled peptide steroid receptor coactivator
(SRC2-3). Increasing amounts of VDR-LBD purified under different conditions (Table-
2) were used in the presence of the ligand LG190178. The data were fit to a sigmoidal

dose-response curve, and Kd values for P-1 B-1 4/4/11 and P-1 B-1 4/21/11 are 89.07 ± 8 nM and 70.83 ± 7 nM respectively.
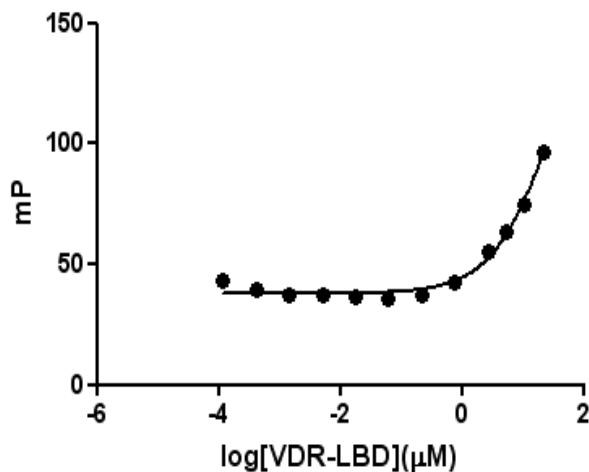
Figure 14 Inactive VDR-LBD Protein. A fluorescence polarization assay employing labeled coregulator peptide SRC2-3 in the presence of the ligand LG190178 and increasing concentrations of VDR-LBD. This protein provided by Dr. Arnold exhibited no saturation at higher protein concentrations. Therefore, a binding constant could not be calculated.

An example of the binding isotherms for the VDR-LBD protein with coregulator peptide SRC2-3 using this fluorescence polarization assay is shown in **figure-13.** This graph shows the fluorescence polarization graphs for two VDR-LBD/Protein-1/Batch-1(s) purified on two different days 4/4/11 and 4/21/11, respectively. The binding of VDR-LBD with fluorescently labeled peptide steroid receptor coactivator (SRC2-3) with Alexa fluor-647 is saturable, exhibiting a plateau with the increasing protein concentrations. The non-linear regression resulted in dissociation constants of 89.07 ± 8 nM (4/4/11) and 70.83 ± 7 nM (4/21/11), respectively. The hill slope of the two protein fractions were 1.00 for 4/4/11 and 1.02 for 4/21/11. We concluded that both proteins are highly functional if compared with the literature values of 930±170 nM [24]. Additionally

no cooperativity of binding was observed. In contrast, **figure-14** shows incomplete

saturation of the signal at higher concentration for the protein provided by Dr. Arnold.

Based on the missing saturation we were not able to calculate a binding constant.

Therefore, this protein has only a very weak interaction with the coregulator SRC2-3.

Table 3 Summary of binding constants between SRC2-3 and VDR-LBD generated with different purification conditions.

Protein-1 $(4\text{-}5^0C)$	Batch no.	Date of purification	K_d (nM)	Average (nM)	S.D. (nM)
1	Batch-1	4/4/2011	89.07		
2	Batch-1	4/21/2011	70.83	73.9	32.1
3	Batch-1	5/20/2011	105.3		
4*	Batch-1	7/14/2011	30.7		
5	Batch-2	4/4/2011	294.6		
6	Batch-2	4/21/2011	168.9	197.3	64.8
7	Batch-2	5/20/2011	163.7		
8	Batch-2	7/14/2011	162.2		
Protein-2 $(4\text{-}10^0C)$					
9	Batch-1	4/4/2011	75.81		
10	Batch-1	4/21/2011	38.24	54.2	19.3
11	Batch-1	5/20/2011	65.32		
12*	Batch-1	7/14/2011	37.7		
13	Batch-2	4/4/2011	57.73		
14	Batch-2	4/21/2011	164.9	92.0	49.6
15	Batch-2	5/20/2011	63.94		
16	Batch-2	7/14/2011	81.66		

Protein-3 $(4\text{-}15^0\text{C})$	Batch no.	Date of purification	K_d (nM)	Average (nM)	S.D. (nM)
17	Batch-1	5/20/2011	86.65		
18*	Batch-1	7/14/2011	37.77	62.2	34.5
19	Batch-2	5/20/2011	183.1	182.3	1.0
20	Batch-2	7/14/2011	181.6		
Protein-4 $(4\text{-}20^0\text{C})$					
21	Batch-1	5/20/2011	221.5		
22*	Batch-1	7/14/2011	34.44	127.9	132.2
23	Batch-2	5/20/2011	366.5	367.3	1.2
24	Batch-2	7/14/2011	368.2		

*ice bath was used for cooling during sonication

We found that all 24 different samples were able to recruit the fluorescently labeled SRC2-3 peptide in the presence of LG190178 based on the sigmoidal curves shown in **figure-13** and **figures 27-37** in **Appendix.** The binding affinities (K_d) for the corresponding fluorescence polarization curves for proteins 1-4 and batch-1 and batch-2 are shown in **table-3**.

We also found that the binding affinities of the batch-2 samples had higher dissociation constants compared to the batch-1 protein samples, for instance for protein 1, batch 1 the average was 73.9 nM compared to batch-2, which average K_d value was 197.3 nM. These differences can be due to the proteases present in the second batch of purifications, which can be degrading the proteins and therefore, affecting the binding affinity.

We analyzed the binding affinity results for a particular purification date 7/14/2011 for batch-1 proteins (**table-3**). There was an exception made during sonication on that particular day because of the warm weather. When we recorded the temperature

of the protein solution after sonication for proteins 1-4 while employing the specified sonication times, we noticed a higher temperature than usual. Therefore, we decided to repeat the experiment using an ice-salt mixture for all the subsequent sonication cycles for proteins 1-4. All K_d values measured for these samples were between 30.7 and 37.7 nM.

In general, we found a relatively high standard deviation, which reflects the difficulties to standardize protein production. Nevertheless, we can conclude that the temperature during purification has a large effect on the binding affinity between VDR-LBD and coregulator peptide SRC2-3.

3.4 Fluorescence Polarization Assay Conclusion

The optimal purification conditions for expressing and purifying the VDR-LBD protein with the highest affinity towards coactivator peptide SRC2-3 are as follows: Firstly, 30 seconds of sonication at 40% amplitude with 5 seconds of pulse and 5 seconds of rest for three cycles is sufficient for cell lysis. Prolonged sonication does not further increase the yield of VDR-LBD protein. Secondly, an ice-salt mixture to cool the sample while sonicating is essential in order to obtain highly functional VDR-LBD protein (K_d = < 50 nM). Thirdly, batch-1 purification should be employed for the best results because batch-2 purification resulted in less functional protein.

The recombinant human VDR has previously been expressed [24] in the *E.coli* , using the MBP as an affinity tag. The K_d value for peptide SRC2-3 was reported 840 nM [24] and our K_d values range from 30.7-368.2nM suggesting a highly functional protein

with tight binding. The improvements might be due an overall better methodology and technique for the expression and purification of VDR-LBD-MBPmt protein.

4. Thermofluor Stability Assay

4.1 Introduction Thermofluor Assay

The Thermofluor stability assay also known as the thermal shift assay was performed to measure the stability of the purified VDR-LBD protein fractions. The stability of the protein was measured by thermally "melting" the protein via heat, in the form of increasing temperature. The fluorescence based thermofluor stability assay was developed by Pantoliano [39], with a basis for the method is that folded and unfolded proteins can be distinguished through exposing the protein to a hydrophobic fluoroprobe such as Sypro Orange. Thermally induced unfolding is an irreversible unfolding process following a typical two-state model with a sharp transition between the folded and unfolded states. The midpoint of temperature of the protein-unfolding transition is referred to as the T_m [40].

This assay takes advantage of the fact that the fluorescence of protein-binding dye such as Sypro Orange, increases with increasing hydrophobicity of it's environment. In this assay a fluorescent dye Sypro orange was added to the protein solution and the temperature of the solution was raised while monitoring the fluorescence of the dye. As the increasing temperature forces the protein to unfold and exposes the normally buried

hydrophobic residues, the fluorescence of the dye increases in response to the increased exposure of hydrophobic surface. The increasing temperature eventually causes the folded, globular protein to unfold or melt. The temperature at the midpoint of this melting transition or T_m is monitored for protein stability studies [41].

There are two great advantages of using the thermofluor stability assay. The first advantage is that this assay is a high-throughput assay, which can be performed for screening a lot of different conditions such as different buffers using a real time PCR (RT-PCR) instrument. This method was adapted in 2001, for high-throughput screening and it can be performed in a 96-well plate. The second advantage is that it only takes 30 minutes for one experiment. Therefore, to take advantage of the high-throughput method, this assay was used to screen the protein samples in a 96-well plate[39].

4.2 Determination of the stability of BSA using the thermofluor stability assay in order to establish the condition of the assay.

The thermofluor assay was performed to investigate the stability of the MBP-VDR-LBD protein. The melting temperature (T_m) was monitored for bovine serum albumin protein (BSA) as a positive control and the purified VDR-LBD protein. The thermofluor assay was performed using the Real Time Polymerase Chain Reaction (RT-PCR) instrument and a fluorescent Sypro Orange dye.

A solution of 50X Sypro Orange dye was prepared from a 5000X stock solution (Purchased from Invitrogen). In order to prepare the 50X Sypro Orange dye solution, 1.2 µL of the dye were added from the 5000X stock solution and mixed with 119 µL of

MilliQ H_2O for a final volume of 120 µL, the diluted dye solution was mixed by pipetting.

Next, the bovine serum albumin (BSA) protein-dye solution was prepared to be used as a positive control. A 30 µM BSA protein solution was prepared in a 1.5 ml tube by combing 59.85 µL of 45.11 µM BSA, 30.15 µL of Millipore H_2O, and 10 µL of 50X Sypro Orange dye giving a final volume of 100 µL. 20 µL of the protein-dye solution was added in quadruplets in a 96-well plate (Eppendorf Twin.Tec PCR Plates). **Figure-15** shows the melting curve of BSA measured by a thermofluor stability assay. The mean T_m was 66.5 ^{0}C with a standard deviation of 0.6.
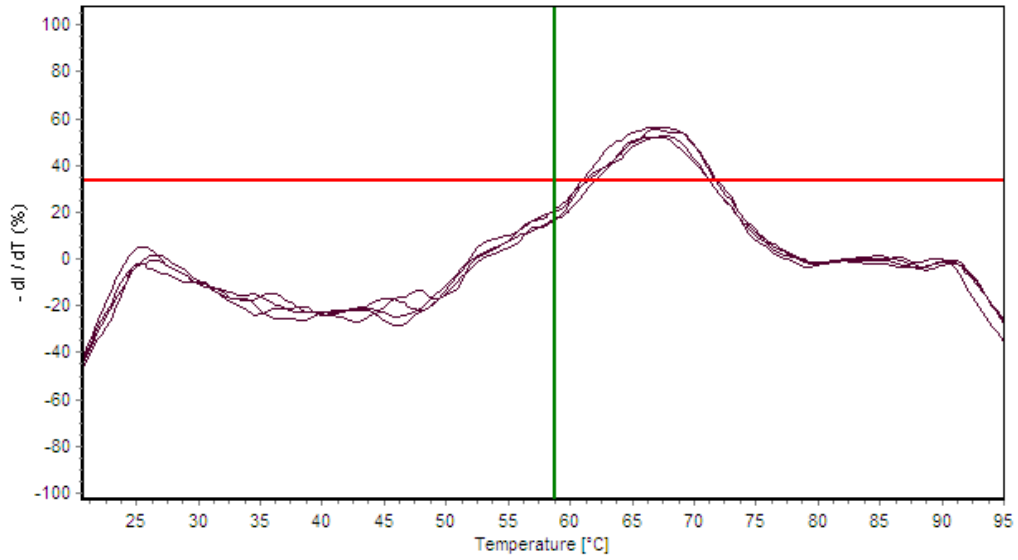
Protein and Concentration	Ex-1 $T_{m\,in}\,{}^0C$	Ex-2 $T_{m\,in}\,{}^0C$	Ex-3 $T_{m\,in}\,{}^0C$	Ex-4 $T_{m\,in}\,{}^0C$	Mean $T_m\,in\,{}^0C$	Standard deviation
BSA 30uM	67.3	66.5	65.9	66.4	66.5	0.6

Figure 15 Thermofluor melting curve of BSA. The plot of the derivative of fluorescence intensity over time vs. the temperature. The maximum value represents the midpoint of the unfolding transition, or Tm. The thermofluor assay was employed in quadruplets for the BSA protein as a positive control. The Tm values for the four replicates are shown in the table and the mean Tm is shown at 66.5 0C with a standard deviation of 0.6.

4.3 Determination of the stability of inactive VDR-LBD using the
Thermofluor Stability Assay

Next, the VDR-LBD protein-dye solution was prepared by using the inactive VDR-LBD protein provided by Dr. Arnold. A 30 µM inactive VDR-LBD protein solution was prepared in a 1.5 ml tube by combining 48.44 µL of 55.73 µM inactive VDR, 41.56 µL of VDR-FP buffer containing 25 mM PIPES, 50 mM NaCl (pH 6.75). 10 µL of 50X Sypro Orange dye was added to the protein-buffer solution for a final volume of 100 µL. 20 µL of the protein-dye solution was added in quadruplets in a 96-well plate (Eppendorf Twin.Tec PCR Plates). 20 µL of VDR-FP buffer was added in quadruplets to the 96-well plate in each well as a negative control. 18 µL of VDR-FP buffer and 2 µL of Sypro Orange dye were added to each well in the 96-well plate in quadruplets for the baseline determination.

Next, the 96-well plate was sealed with Eppendorf real-time PCR optical adhesive film to prevent evaporation from the thermal melt. The film was applied very firmly on the well plate to prevent any gaps or spaces between each well. The 96-well plate was then centrifuged at 1000 rpm for 1 minute at room temperature to ensure mixing. The well plate was heated in the Master Cycler Real Plex PCR instrument from 20^0C to 95^0C using filter 2, which corresponds to the excitation/emission wavelength at 520/550nm referred to as SYBR.
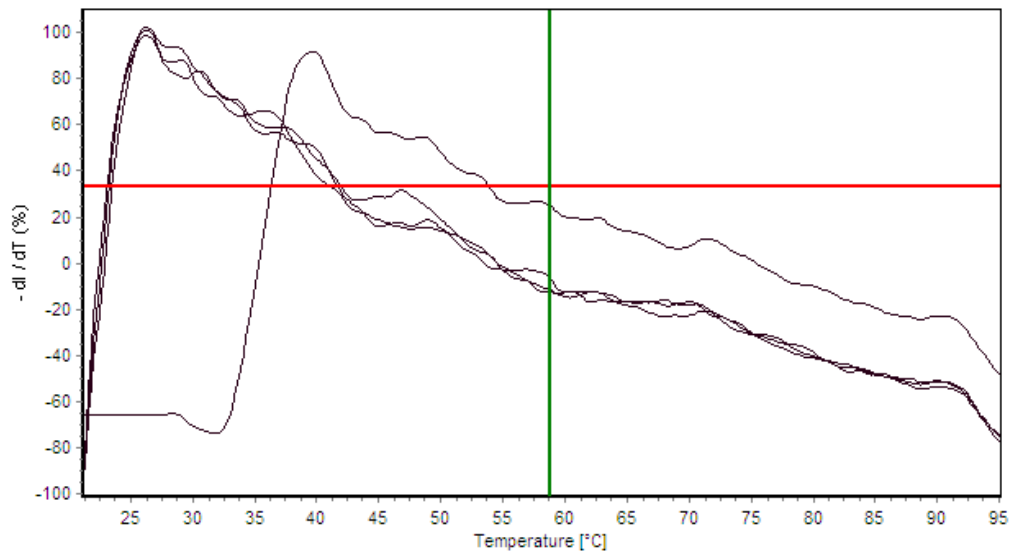
Protein and Concentration	Exp-1 $T_{m\ in}\ ^0C$	Exp-2 $T_{m\ in}\ ^0C$	Ex-3 $T_{m\ in}\ ^0C$	Ex-4 $T_{m\ in}\ ^0C$	Mean $T_m\ in\ ^0C$	Standard deviation
Inactive VDR-LBD 30 µM	26.3	39.5	26.2	26.3	29.6	7.7

Figure 16 Thermofluor stability assay with inactive VDR-LBD. The derivative of the fluorescence intensity over time is plotted against the temperature. The maximum value represents the midpoint of the unfolding transition, or Tm. The thermofluor assay was employed in quadruplets. The Tm values for the four replicates are shown in the table and the mean Tm is shown at 29.6 0C with a standard Deviation of 7.7.

The data shown in **figure-16** for the melting curve of the VDR-LBD protein did not show consistent results as shown in the graph. The four replicates has a T_m ranging from 26.2-39.5^{0}C with a mean T_m of 29.6^{0}C and standard deviation of 7.7, indicative of the inconsistency between the replicates. Also, the T_m values are very low compared to the reported T_m of 53^{0}C for VDR-LBD via Circular Dichroism Spectroscopy [42]. We thought that the buffer used to store the VDR-LBD protein consists of the detergent NP-40 in the dialysis buffer, which might be the cause of the low T_m values and the

inconsistency. Therefore, we tried to perform dialysis using 4L of the VDR-FP buffer containing 25 mM PIPES, 50 mM NaCl pH 6.75. 3 ml of the inactive VDR-LBD protein was dialyzed overnight using the 3 ml volume 10K Slide-a-Lyzer G2 dialysis cassettes (purchased from Pierce).

4.4. Determination of the stability of dialyzed inactive VDR-LBD using the Thermofluor Stability Assay

Hypothesis: We propose that the detergent nonyl phenoxypolythoxyethanol (NP-40) present in the protein solution of inactive VDR-LBD might be causing the low melting temperature depicted in **figure 16**. Therefore, the inactive VDR-LBD protein was dialyzed in the FP buffer containing 25 mM PIPES and 50 mM NaCl to remove the detergent from the protein solution. The thermofluor assay was again performed after dialyzing the protein using the FP buffer in quadruplets. The results are shown in **figure-17.**
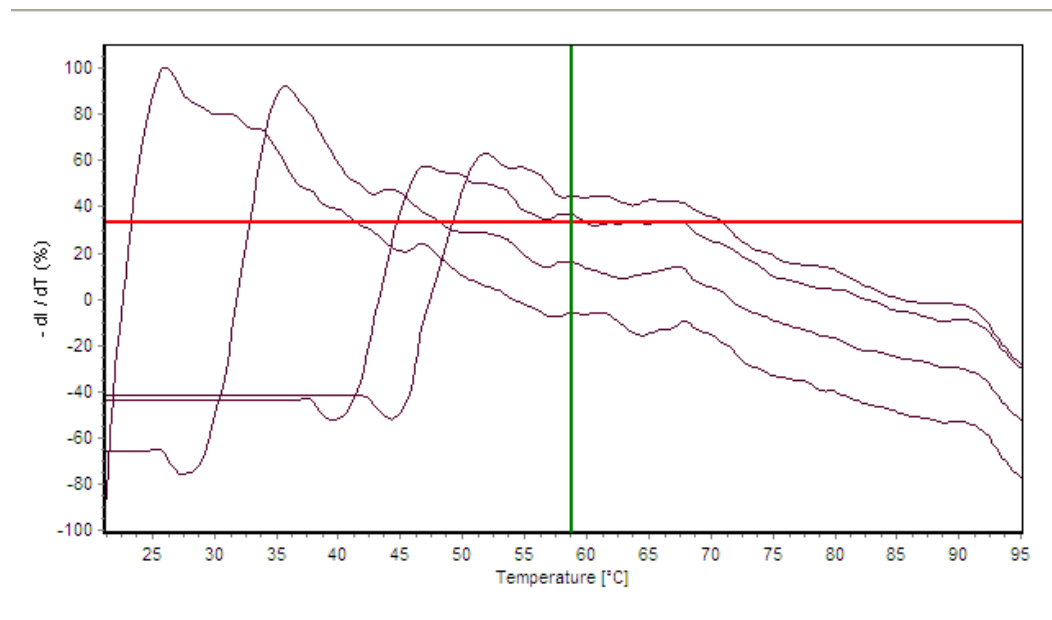
Protein and Concentration	Exp-1 $T_{m\,in}\,^0C$	Exp-2 $T_{m\,in}\,^0C$	Ex-3 $T_{m\,in}\,^0C$	Ex-4 $T_{m\,in}\,^0C$	Mean $T_m\,in\,^0C$	Standard deviation
Inactive Dialyzed VDR-LBD 30uM	26.1	35.8	52.0	46.5	40.1	8.2

Figure 17 Thermofluor assay with dialyzed inactive VDR-LBD protein. The graph shows the relationship between the derivative of the fluorescence intensity over time vs the temperature. The maximum value represents the midpoint of the unfolding transition, or Tm. The thermofluor assay was employed in quadruplets. The Tm values for the four replicates are shown in the table and the mean Tm is shown at 40.1°C with a standard Deviation of 8.2°.

The data in **figure-17** again shows inconsistency within the replicates with the T_m ranging from 26.1-52.0°C and a mean T_m of 40.1°C with a higher standard deviation of 8.2 compared to the undialyzed protein. Obviously, dialyzing the protein did not help the results. A more detailed literature research revealed that NP-40 cannot be dialyzed due to it's unique polymeric structure [43]. Therefore, an alternative method should be applied to separate VDR-LBD and NP-40.

4.5. Determination of the stability of buffer-exchanged inactive VDR-LBD using the Thermofluor Stability Assay

Hypothesis: We propose that the detergent Nonyl phenoxypolythoxyethanol (NP-40) can be removed by specialized spin columns in order to obtain VDR protein with consistent melting points when measured with a thermofluor assay.

The VDR-LBD protein should give us a T_m value comparable with the literature value after separation from NP-40. The spin columns contain resin which enables the removal of non-ionic detergents such as the NP-40 from protein solutions. Instructions from the manufacturer were used to remove the detergent. The spin column was centrifuged for 1 minute at 1500xg to remove the storage buffer. Next, 0.4ml of the VDR-FP buffer was added to the spin column and centrifuged at 1500xg for 1 minute. The flow-through was discarded and this process was repeated again. Next, 100 µL of the inactive VDR-LBD containing the NP-40 detergent was added to the spin column and incubated for 2 minutes. The spin column centrifuged at 1,500xg for 2 minutes to collect the detergent-free sample. The thermoflour assay was repeated again after the using the spin columns data shown in **figure-18**.
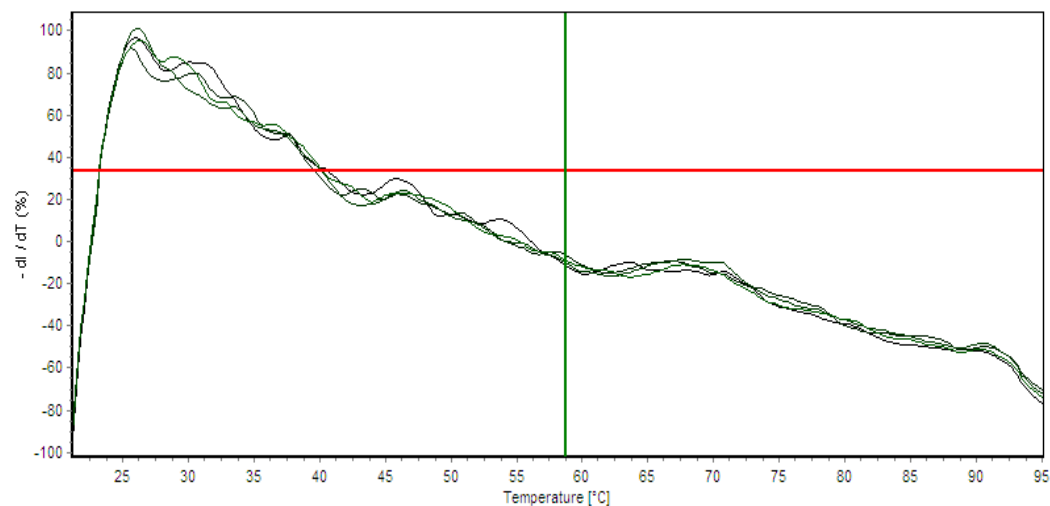
Protein and Concentration	Exp-1 $T_{m\,in}\,^0C$	Exp-2 $T_{m\,in}\,^0C$	Ex-3 $T_{m\,in}\,^0C$	Ex-4 $T_{m\,in}\,^0C$	Mean T_m in ^0C	Standard deviation
Inactive Buffer exchanged VDR-LBD 30uM	26.1	25.8	26.1	26.4	26.1	0.2

Figure 18 Thermofluor assay with inactive VDR-LBD protein after buffer exchange. The graph shows the relationship between the derivative of the fluorescence intensity over time vs the temperature. The maximum value represents the midpoint of the unfolding transition, or Tm. The thermofluor assay was employed in quadruplets. The Tm values for the four replicates are shown in the table and the mean Tm is shown at 26.1°C with a standard deviation of 0.2°C.

The T_m values obtained for the inactive VDR-LBD after NP-40 removal using the spin columns described above are ranging from 25.8-26.4°C. The mean T_m was 26.1°C with a standard deviation of 0.2 indicating that using the spin column only helped the data to be more consistent than the un-dialyzed protein depicted in **figure 16**. Still, the melting point is significantly lower than the reported literature value.

4.6. Determination of the stability of active VDR-LBD protein batches using a thermofluor stability assay

The thermofluor stability assay was also performed with 24 different samples (undialyzed) of the active VDR-LBD in duplicate and the results are shown in **figure-19.**
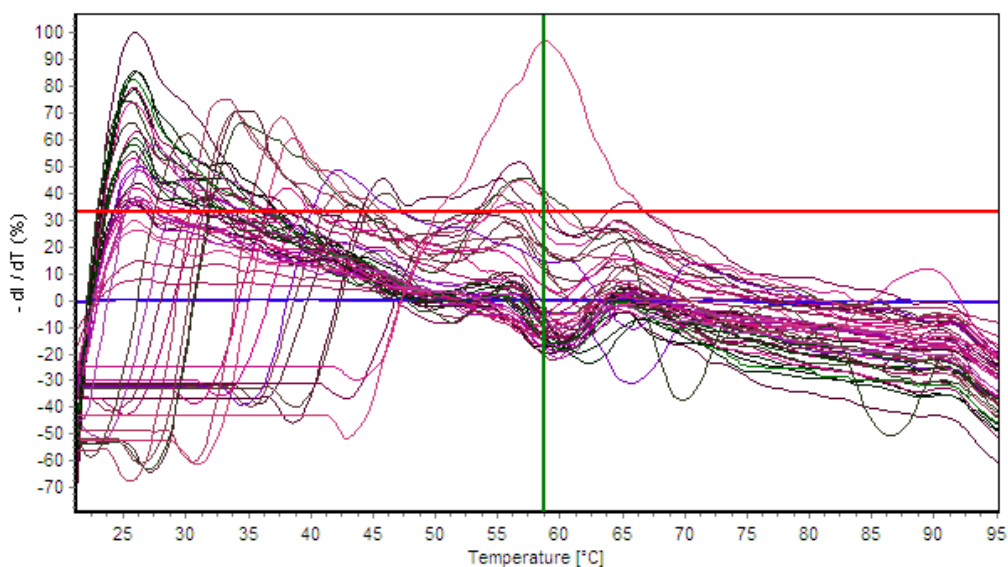
Figure 19 Thermofluor assay with 24 active samples of VDR-LBD protein. The graph shows the relationship between the derivative of the fluorescence intensity overtime vs the temperature. Thermofluor assay was employed in duplicates for the 24 active samples of VDR-LBD protein, the midpoint of the unfolding transition, or Tm was monitored.

The results in **figure-19** showed a wide range of melting temperature for the different VDR-LBD batches described in chapter 2. The duplicates were inconsistent. The highest midpoint transition T_m value is shown at 58°C for the protein sample P-1 B-1 7/14/2011.

4.7 Thermofluor Stability Assay Conclusion

The thermofluor assay was performed to determine the stability of the VDR-LBD protein. The Bovine Serum Albumin (BSA) protein was used as a positive control and the BSA protein worked successfully showing the mean T_m of 66.5°C. The previously reported value of thermally induced unfolding for BSA with a T_m of 59°C performed via differential Scanning Calorimetry is comparable with our value of 66.5°C [44].

However, the melting temperatures for VDR-LBD proteins were too low, which was attributed to additives such as NP-40. Detergents have a destabilizing effect on reversible interactions which might obscure the signal generated by the melting of the protein of interest. Thus, detergents are only sparingly tolerated by the thermofluor assay [41] and therefore showing low melting temperature ranging from 26.2-39.5°C with a mean T_m of 29.6°C and a standard deviation of 7.7. The VDR-LBD protein was dialyzed in the VDR-FP buffer and the thermofluor assay was repeated the T_m values ranged from 26.1-52.0°C and a mean T_m of 40.1°C with a higher standard deviation of 8.2°C, indicating that dialyzing the protein did not work. Another attempt was made to remove the NP-40 detergent by using the spin columns yet, the results exhibited very low melting temperature ranging from 25.8-26.4°C and a mean T_m of 26.1°C with a standard deviation of 0.2°C. Therefore, we concluded that the thermofluor assay worked

successfully on the BSA protein but it was not successful with the VDR-LBD protein due to the additives such as NP-40 that might be present in the VDR-LBD protein solution. These additives could not be removed from the solution using dialysis or the detergent removal spin columns and caused deleterious effects for VDR-LBD protein. The detergent may have affected the hydrophobicity of the solution and obscured the signal of Sypro Orange dye. Therefore, we decided to measure the thermal stability of the VDR-LBD protein with another assay using the Differential Scanning Calorimetry in which no dyes are employed.

5. Differential Scanning Calorimetry

5.1 Introduction

Differential Scanning Calorimetry (DSC) is a powerful technique for determining thermodynamic stability of biomolecules such as proteins. The DSC experiment allows to monitor the unfolding or phase transitions of proteins which provides the information about their thermodynamic stability [45].

The thermodynamic stability of a protein is the operational stability in terms of the strength of interactions maintaining a native three-dimensional structure and can be described as equilibrium between the folded and unfolded state of protein. The native structure of macromolecules such as proteins, are stabilized by cooperation of many weak

forces including hydrogen bonds, hydrophobic interactions, and electrostatic interactions [46].

Upon protein heating, enough energy is provided by the system to overcome these weak forces resulting in a conformational or phase transition of the protein. The parameters that are generally used to characterize the stability of a protein includes the Gibbs free energy (ΔG) [44],[46]. The Gibbs free energy is temperature dependent, and it can be evaluated by using the thermodynamic relationship shown in Equation-1. ΔG is reflected by the enthalpic (ΔH) and the entropic (ΔS) change and these relationships and can be quantified by using Differential Scanning Calorimetry.

$$\Delta G = \Delta H - T\Delta S - \text{Equation -1}$$

Differential Scanning Calorimetry (DSC) measures the enthalpy ΔH of protein unfolding due to heat denaturation. DSC is a powerful technique that directly measures the heat of unfolding and provides information about the stability of a protein. DSC is a label-free technique, in which no dye is required to determine the T_m, heat capacity (ΔC_p), Enthalpy (ΔH), and Entropy (ΔS) associated with protein unfolding [46].

During a thermal melt, a protein in solution is in equilibrium between the native (folded) and the denatured (unfolded) states. When 50% of the protein in solution is unfolded or melted, the molar heat capacity (C_p, max) is at maximum. This is defined as the melting temperature or the thermal midpoint transition (T_m). The T_m allows for an experimental window into the stability of the protein. An increase in the T_m in a different buffer demonstrates the higher stability of the protein [45] in that buffer, [46]. Likewise, a decrease in T_m demonstrates instability.

The DSC can also determine the change in molar heat capacity (ΔC_p). The molar heat capacity is the amount of heat required to change the temperature of one mole of a substance by one degree °C [47]. The thermal denaturation of a protein transitioning from native to unfolded state is associated with extensive heat absorption over a temperature range that depends on the solvent conditions and results in a significant heat capacity increase [48].

Another parameter that can be measured using the DSC during an unfolding transition of proteins is the change in enthalpy (ΔH). The calorimetric enthalpy is the energy of unfolding. ΔH is calculated from the area under the peak shown in **figure-20** of the unfolding transition from the integral of the excess heat capacity function shown in equation-2, where T_0 is the temperature of the folded and T_u is the temperature of the folded state [45].

$$\Delta H = \int_{T0}^{Tu} Cp(ex)dT \text{ Equation-2}$$

Another transition parameter that can be quantified is the change in entropy (ΔS). Entropy is a measure of randomness or disorder in a closed system. The overall entropy change for unfolding transition is define by Equation-3 [45]. However, for a well-defined two-state transition from folded to unfolded, the Gibbs free energy (ΔG) is zero at T_m, then the entropy change (ΔS) is simply $\Delta S=\Delta H/T$. **Figure-20** shows a representative graph of thermal unfolding of a monomeric protein and how the different variables are calculated.

$$\Delta S = \int_{T0}^{Tu} \frac{Cp(ex)}{T} dT \text{ Equation-3}$$
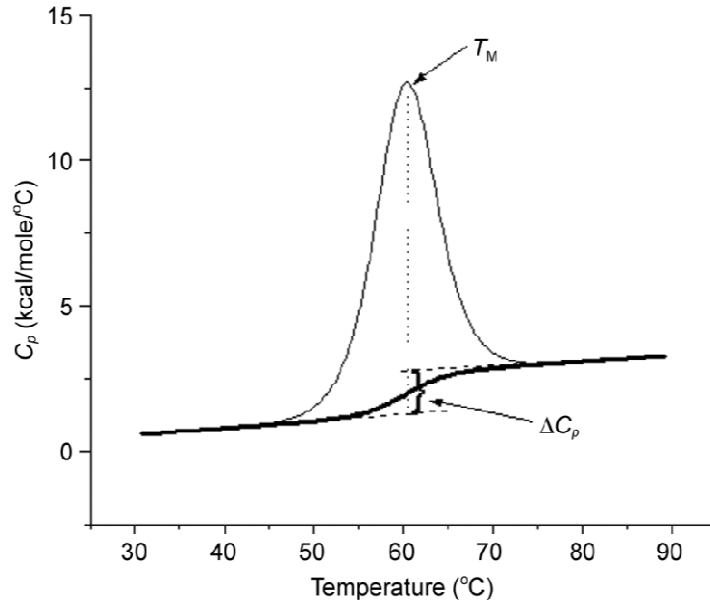
Figure 20 Thermal unfolding of a representative monomeric protein. In this graph temperature is plotted as a function of x-axis and the excess heat capacity is plotted as a function of y-axis. From this graph Tm, ΔH, ΔCp can be measured. The maximum of heat capacity is shown at the Tm of 600C. The dashed line is a computer generated "progress" baseline, the area of the heat absorption between the peak and the progress baseline represents the calorimetric enthalpy ΔH. The dashed lines are the linear extrapolations of the pre-post transition baselines into the transition region, the difference between these values is the ΔCp 46.

The thermal scanning of protein solutions leads to transitions from native to intermediate, partially folded states and finally to the completely denatured state of the protein. For protein unfolding, the thermally induced transition can approach a two-state process. The two-state process is the transition between the native and the unfolded state [45].

In order to study the transitions, these calorimetric studies require a highly sensitive DSC instrument such as the Nano series TA DSC used in this experiment. The instrument must be able to respond to the small energy changes associated with unfolding

50

at low protein concentrations. The high sensitivity is achieved by using the differential

power compensation between the reference and the sample cell, and a carefully designed

method to control the temperature as well as the scanning rate [45]. The measurement cells

in which the sample and the reference is injected are surrounded by a shield [49], that

controls the temperature of scanning in order to run an adiabatic scan [50]. No heat flows

from or to the cells from the surrounding during scanning the temperature of the cells [45].

5.2 Methods and Material for DSC

The Differential Scanning Calorimetry (DSC) was performed to determine the

stability of the VDR protein in relationship to its ability to bind the coregulator peptide

SRC2-3 and to understand the transitions and the thermal behavior of VDR.

In order to test the stability, two samples in 1.5 ml tubes were prepared using the

fluorescence polarization (FP) Buffer containing 25 mM PIPES and 50 mM NaCl at pH

6.75. One sample tube contained 1 ml of the FP buffer referred to as the reference and the

other tube contained 1ml 30 μM of VDR protein in the FP buffer. Both of the sample

vials were first degassed to prevent any dissolved gasses coming out of the solution and

to prevent the formation of bubbles. The bubbles may cause problems with stabilizing the

instrument and erroneous data. Therefore, it is very important to degas the samples before

injecting into the DSC instrument. To degas the samples, a small magnetic stir bar was

inserted into both the reference tube and the protein sample tube. Both of the tubes were

then placed into a vacuum degassing compartment (TA-Degassing Station). Both of the

samples were degassed for 15 minutes with stirring at 1000 rpm and pressure 300 mmHg

at room temperature. The Nano series TA DSC instrument contains two symmetrical

capillary cells, one capillary cell for the reference (labeled R) and another one for the sample (labeled S). Each capillary contains two openings referred to as cell-1 and cell-2 for the reference and for the sample. Before loading the samples, all the cells were first rinsed with distilled water (undegassed) and then with FP buffer (undegassed).

To load the samples, a 1 ml pipette was used to inject the reference containing the FP buffer first. The degassed reference FP buffer was aspirated carefully from the 1.5 ml tube without producing any bubbles. One of the reference cells (cell-1) were covered with an empty 1 ml pipette tip and 1 ml of the reference buffer was pipetted in and up and down into cell-2. Pipetting up and down, the reference comes out into cell-1, reduces bubbles, and fills the capillary cell. The pipette tip in cell-2 was very carefully disposed once the reference has entered cell-1. There was a meniscus formed on top of both cell 1 and cell 2 after ejecting the pipette tips from both of the cells. Cell-1 is then covered with a small rubber cap after wetting the cap with 1 drop of water. This process is repeated for injecting the protein sample into the sample capillary cell. After injecting both the reference and the protein sample a meniscus is visible on top of the cells. All the cells are then covered with a metal cap twisted very tightly, to ensure an adiabatic system. The DSC instrument was then turned on and stabilized at -0.2μW at 25 ^{0}C for 15-20 minutes. Improper stabilization may cause false data. There are two heating and cooling cycles involved for each run. The DSC instrument is set to increase the temperature from 20-100 ^{0}C at the rate of 1.5^{0}C/minute at 3 atm. The instrument can only control the heating process and the cooling process must occur naturally. This heating and cooling process was then repeated for the second cycle. The experiment takes approximately 5-6 hours to complete for each protein sample.

5.3 Differential Scanning Calorimetry Results

Differential Scanning Calorimetry (DSC) was used to determine the stability of the VDR-LBD protein in relationship to its ability to bind the coregulator peptide SRC2-3 and to study the thermally induced conformational transition. DSC was used to directly measure the heat associated with transitioning from the native to unfolded state. DSC is the only method for the direct determination of ΔH. DSC measures the excess heat capacity of a solution C_p of the protein as a function of temperature. The transition is recognized as a sharp peak centered at the melting transition T_m and the maximum C_p occurs directly at T_m. In a single experiment, DSC can also provide thermodynamic information such as the ΔH and ΔS[44].

In order to establish the condition of the DSC experiment, a 30 μM solution of Bovine Serum Albumin (BSA) was loaded on the DSC. Graph of the thermal unfolding of BSA is shown in **figure-21**.
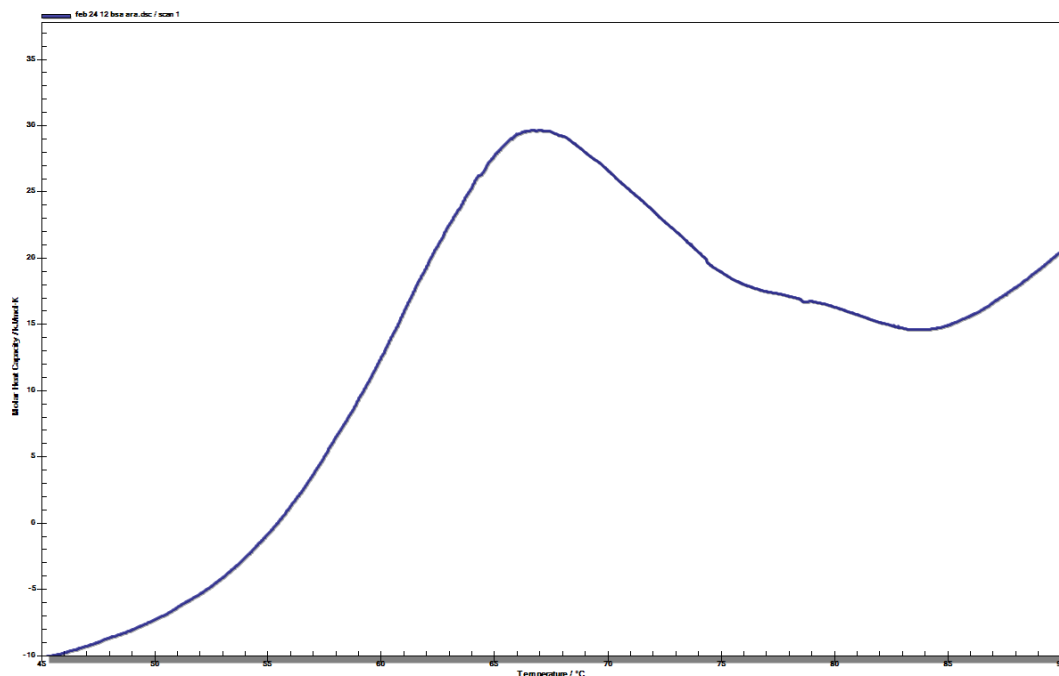
Figure 21 DSC Thermogram for BSA Protein. DSC thermogram observed during the thermal unfolding of Bovine Serum Albumin. In this graph temperature in °C is plotted as a function of x-axis and the excess heat capacity Cp in kJ/mol.K is plotted as a function of y-axis. The BSA shows a typical two-state thermally induced unfolding. The peak at which the maximum heat capacity is observed is the melting transition Tm of 66.31 °C. The area under the peak represents the calorimetric enthalpy ΔH shown at 312.88 kJ/mol. ΔS is shown at 0.92 kJ/molK.

The excess heat capacity of the protein solution C_p (Y-axis) is plotted as a function of temperature (X-axis). The BSA shows a typical two-state transition going from folded to unfolded state and it is recognized at the maximum heat capacity centered at the T_m of 66.31°C which is in a close agreement with the thermofluor stability assay which showed a T_m of 66.5°C (**figure-15**) indicative of the successful DSC run. DSC also measured the thermodynamic values of ΔH at 312.88 kJ/mol, and ΔS 0.92 kJ/molK shown in **figure 21**.

In order to determine the relationship between the functionality and the stability of the VDR-LBD protein using the DSC, six protein samples were chosen out of the 24

purified protein samples. We selected 2 samples with low K_d values, 2 samples for the medium K_d values and 2 samples for the high K_d values. The determined melting curves are presented in **figures 22-24** together with the melting curve for the inactive VDR protein provided by Dr. Arnold.
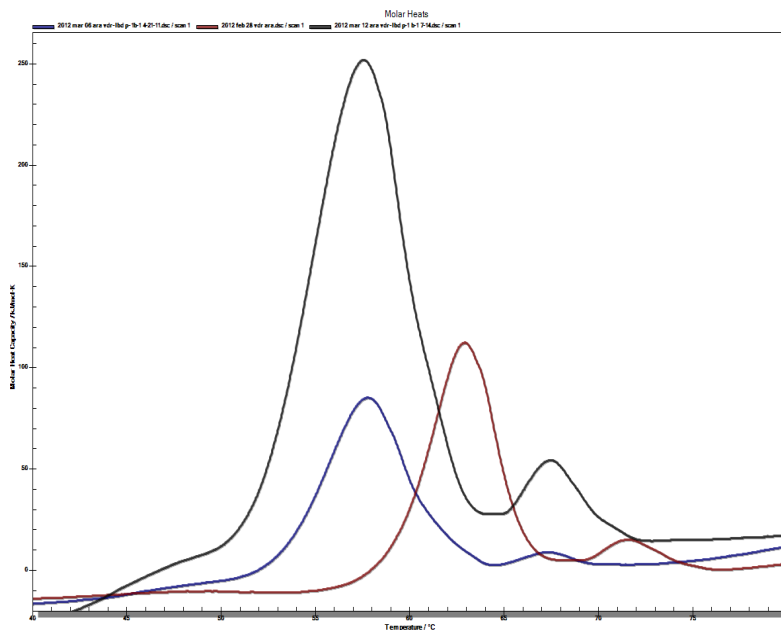
 Figure 22 DSC Thermograph for VDR-LBD proteins with small K_d values. DSC thermogram observed during the thermal unfolding of VDR-LBD is showing an overlay of three protein samples, Protein-1 B-1 7/14/2011, Protein-1 B-1 4/21/2011, and Inactive VDR-LBD Protein. The peak at which the maximum heat capacity is observed is the melting transition Tm of 62.9°C for the inactive VDR. The two VDR samples of Protein-1 B-1 7/14/2011, Protein-1 B-1 4/21/2011 exhibited Tm values of 57.62°C and 57.77°C, respectively. The data for all three samples are shown in the table below corresponding to the color of each peak.

VDR-LBD Protein	K_d in nM	T_m in ^{0}C	ΔH in kJ/mol	ΔS in kJ/mol.K
Protein-1 B-1 7/14/2011	30.7	57.62	1410.15	4.26
Protein-1 B-1 4/21/2011	70.83	57.77	419.54	1.27
Inactive Protein	>32000	62.9	477.26	1.42

The DSC graph of the thermal unfolding of VDR-LBD for the samples that have a low K_d values 30.7 nM and 70.83 nM for samples Protein-1 B-1 7/14/2011, Protein-1 B-1 4/21/2011, respectively are shown in **figure-22**. **Figure-22** shows an overlay of the two active proteins and the inactive protein. The peak at which the maximum heat capacity is observed is the melting transition T_m of 62.9°C for the inactive VDR is higher than the other two samples of Protein-1 B-1 7/14/2011, and Protein-1 B-1 4/21/2011 with T_m of 57.62 and 57.77°C respectively. It appears the higher melting temperature is an indication for a weak interaction between VDR and coregulator peptide SRC2-3. ΔH and ΔS of all samples were different because protein concentrations used were not the same.
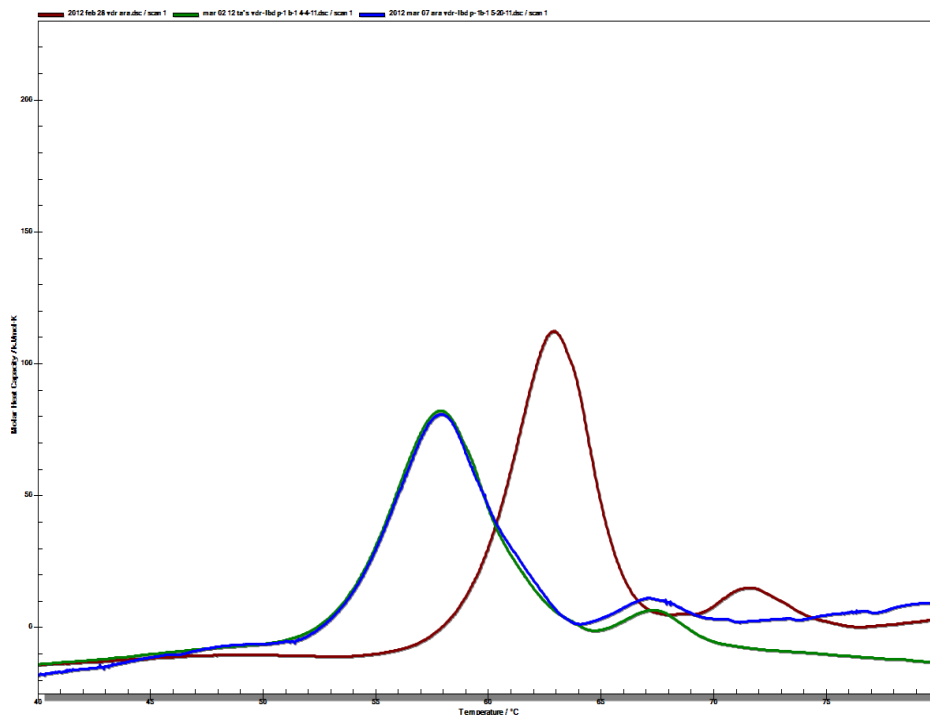
Figure 23 DSC Thermogram for VDR-LBD proteins with medium K_d values. DSC thermogram observed during the thermal unfolding of VDR-LBD is showing an overlay of three protein samples, Protein-1 B-1 4/4/2011, Protein-1 B-1 5/20/2011, and Inactive VDR-LBD Protein. The peak at which the maximum heat capacity is observed is the melting transition Tm of 62.9°C for the inactive VDR. The two VDR samples of Protein-1 B-1 4/4/2011, Protein-1 B-1 5/20/2011 exhibited Tm values of 57.86°C and 57.85°C, respectively. The data for all three samples are shown in the table below corresponding to the color of each peak.

VDR-LBD Protein	K_d in nM	T_m in ^{0}C	ΔH in kJ/mol	ΔS in kJ/mol.K
Protein-1 B-1 4/4/2011	89.07	57.86	440.41	1.33
Protein-1 B-1 5/20/2011	105.3	57.85	408.17	1.23
Inactive Protein	>32000	62.9	477.26	1.42

Next, The DSC graph of the thermal unfolding of VDR-LBD for the samples that have a medium K_d values 89.07 nM and 105.3 nM for samples Protein-1 B-1 4/4/2011, Protein-1 B-1 5/20/2011 respectively are shown in **figure-23**. **Figure-23** shows an overlay of the two active proteins and the inactive VDR protein. The peak at which the maximum heat capacity is observed is the melting transition T_m of 62.9°C for the Inactive VDR is higher than the other two samples of Protein-1 B-1 4/4/2011, and Protein-1 B-1 5/20/2011 with T_m of 57.86 and 57.85°C respectively.
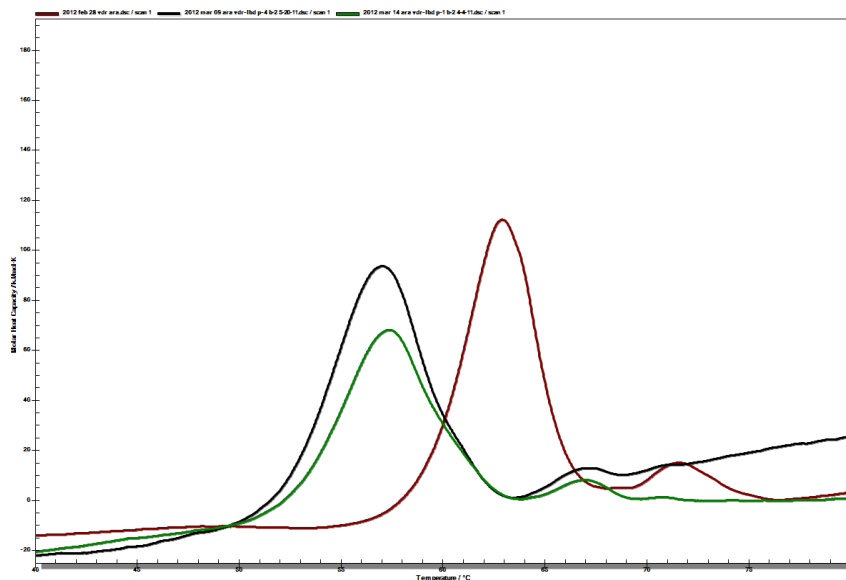
Figure 24 DSC Thermogram for VDR-LBD proteins with high K$_d$ values. DSC thermogram observed during the thermal unfolding of VDR-LBD is showing an overlay of three protein samples, Protein-1 B-2 4/4/2011, Protein-4 B-2 5/20/2011, and Inactive VDR-LBD Protein. The peak at which the maximum heat capacity is observed is the melting transition Tm of 62.9°C for the inactive VDR. The two VDR samples of Protein-1 B-2 4/4/2011, Protein-4 B-2 5/20/2011 exhibited Tm values of 57.280C and 57.03°C, respectively. The data for all three samples are shown in the table corresponding to the color of each peak.

VDR-LBD Protein	K$_d$ in nM	T$_m$ in ^{0}C	ΔH in kJ/mol	ΔS in kJ/mol.K
Protein-1 B-2 4/4/2011	294.6	57.28	399.97	1.21
Protein-4 B-2 5/20/2011	366.5	57.03	471.94	1.43
Inactive Protein	>32000	62.9	477.26	1.42

Finally, two more active VDR-LBD samples with high K_d values were observed during the thermal unfolding of VDR. **Figure-24** shows an overlay of three protein samples, Protein-1 B-2 4/4/2011, Protein-4 B-2 5/20/2011, and the inactive VDR-LBD Protein. The melting transition T_m of 62.9°C for the inactive VDR is higher than the other two samples of Protein-1 B-2 4/4/2011, Protein-4 B-2 5/20/2011 with T_m of 57.28 and 57.03°C, respectively. To compare all DSC data, we compiled all data in **table-4**.

Table 4 Summary of all energies and binding constants of VDR-LBD proteins determined by DSC.

Protein-1	K_d in nM	T_m in ^0C	ΔH in kJ/mol	ΔS in kJ/mol.K
B-1 7/14/2011	30.7	57.62	1410.15	4.26
B-1 4/21/2011	70.83	57.77	419.54	1.27
B-1 4/4/2011	89.07	57.86	440.41	1.33
B-1 5/20/2011	105.3	57.85	408.17	1.23
B-2 4/4/2011	294.6	57.28	399.97	1.21
Protein-4 B-2 5/20/2011	366.5	57.03	471.94	1.43
Inactive Protein	>32,000	62.9	477.26	1.42

5.4 DSC Discussion and conclusion

DSC is a powerful technique for studying thermal transitions of proteins such as VDR-LBD to determine the stability via the melting temperature T_m at which 50% of the molecules are denatured in the solution. DSC not only determines the T_m but can also be used to determine the thermodynamic parameters associated with these changes, such as the ΔH and ΔS in a single experiment.

The thermodynamic parameters were determined for the BSA protein in order to determine the general experimental conditions. We found that BSA showed a two-state

transition with a T_m of 66.31°C, which is in a close agreement with the thermofluor

stability assay, which was T_m of 66.5°C. The confirmation of the T_m by using two

different experiments helped us to determine that the thermofluor assay was not working

with VDR-LBD protein. Therefore, all six protein samples of the active VDR-LBD were

studied using DSC.

All the active protein samples showed the T_m values in a very close range from

57.03-57.62°C, indicative of similar stability. The reported T_m value for the VDR-LBD is

53^0C measured via Circular Dichroism Spectroscopy [42]. The difference of 4°C indicates

that all the active VDR-LBD protein samples measured showed a higher thermal

stability.

According to the data summarized in **table-4,** which shows the values of T_m, ΔH

and ΔS in the order of increasing K_d values of the samples, we found that the inactive-

VDR LBD showed a highest T_m of 62.9°C compared to all the active protein samples. We

also found that the relationship between the binding affinity and the magnitude of the

observed temperature shift is not a correlated for active VDR protein. Nevertheless, a

significant temperature difference was observed for active and inactive VDR protein. The

more stable VDR-LBD protein exhibited a weak interaction with coregulator peptide

SRC2-3, whereas the more active VDR protein was less stable.

6. Final Conclusion

This investigation determines the relationship between sonication times, temperature, functionality and stability of the VDR protein. In this study we showed that increasing the sonication time increased the temperature of the protein mixture during purification even if carried out under cooling using an ice bath (0°C). We showed that this difference in temperature alters the functionality of VDR to interact with coregulator proteins demonstrated by the fluorescence polarization binding assay [51]. Therefore, in this study we showed that using ice-salt mixture (~ -15°C) is highly beneficial and it significantly affects the binding affinity of the VDR-LBD. Therefore, we found that the ideal conditions for purifying the VDR-LBD protein is to use the ice-salt mixture, and sonicate for 30 seconds in 3 cycles.

We also showed that there is no relationship between the functionality and the stability of the VDR-LBD protein, because the inactive protein showed a higher melting temperature (T_m) at 62.9°C compared to the active protein samples which showed the T_m of ~57°C. This demonstrates that there is no relationship between the functionality and the stability of the VDR-LBD protein. An non-functional protein can be highly stable as demonstrated using the Differential Scanning Calorimetry.

7. Future Directions

To obtain the melting temperatures for all 24 purified fractions of VDR-LBD, the thermofluor stability assay was performed; mainly, because of it's high-throughput ability to analyze samples. However, this high-throughput screening method did not give the expected results for the VDR-LBD protein. Further investigations are needed in order to produce VDR-LBD which is pure enough to be measured by a thermofluor assay.

When the Differential Scanning Calorimetry (DSC) experiment was conducted to investigate the stability of the VDR-LBD-MBP protein, a small peak second was also visible, which is probably a different protein present in the solution such as the MBP. A digestion experiment with VDR-LBD-MBP in the presence of Protease Factor Xa enzyme can separate VDR-LBD and MBP. The two proteins can be investigated further by using DSC to determine, if the second small peak on the DSC thermogram is the MBP or another over-expressed protein present in the protein solution.

Additional techniques can be investigated in the future to characterize the behavior of the protein to relate the loss of function to a change of VDR structure. Crystallography is a excellent technique in order to resolve structures of VDR proteins with different degrees of functionality. The knowledge of a three dimensional structure of non-functional VDR might be very interesting in the context of the natural occurrence of this isoform.

8. References

1.   (a) Brumbaugh, P. F.; Haussler, M. R., 1 Alpha,25-dihydroxycholecalciferol receptors in intestine. II. Temperature-dependent transfer of the hormone to chromatin via a specific cytosol receptor. *J Biol Chem* **1974,** *249* (4), 1258-62; (b) Mellon, W. S.; DeLuca, H. F., An equilibrium and kinetic study of 1,25-dihydroxyvitamin D3 binding to chicken intestinal cytosol employing high specific activity 1,25-dehydroxy[3H-26, 27] vitamin D3. *Arch Biochem Biophys* **1979,** *197* (1), 90-5.

2.   Vanhooke, J. L.; Benning, M. M.; Bauer, C. B.; Pike, J. W.; DeLuca, H. F., Molecular structure of the rat vitamin D receptor ligand binding domain complexed with 2-carbon-substituted vitamin D-3 hormone analogues and a LXXLL-containing coactivator peptide. *Biochemistry* **2004,** *43* (14), 4101-4110.

3.   (a) Masuyama, H.; Brownfield, C. M.; St-Arnaud, R.; MacDonald, P. N., Evidence for ligand-dependent intramolecular folding of the AF-2 domain in vitamin D receptor-activated transcription and coactivator interaction. *Mol Endocrinol* **1997,** *11* (10), 1507-17; (b) Hong, H.; Kohli, K.; Garabedian, M. J.; Stallcup, M. R., GRIP1, a transcriptional coactivator for the AF-2 transactivation domain of steroid, thyroid, retinoid, and vitamin D receptors. *Mol Cell Biol* **1997,** *17* (5), 2735-44; (c) Li, H.; Gomes, P. J.; Chen, J. D., RAC3, a steroid/nuclear receptor-associated coactivator that is related to SRC-1 and TIF2. *Proc Natl Acad Sci U S A* **1997,** *94* (16), 8479-84.

4.   (a) Spencer, T. E.; Jenster, G.; Burcin, M. M.; Allis, C. D.; Zhou, J.; Mizzen, C. A.; McKenna, N. J.; Onate, S. A.; Tsai, S. Y.; Tsai, M. J.; O'Malley, B. W., Steroid receptor coactivator-1 is a histone acetyltransferase. *Nature* **1997,** *389* (6647), 194-8; (b) Chen, H.; Lin, R. J.; Schiltz, R. L.; Chakravarti, D.; Nash, A.; Nagy, L.; Privalsky, M. L.; Nakatani, Y.; Evans, R. M., Nuclear receptor coactivator ACTR is a novel histone acetyltransferase and forms a multimeric activation complex with P/CAF and CBP/p300. *Cell* **1997,** *90* (3), 569-80.

5.   Rossetto, D.; Truman, A. W.; Kron, S. J.; Cote, J., Epigenetic modifications in double-strand break DNA damage signaling and repair. *Clinical cancer research : an official journal of the American Association for Cancer Research* **2010,** *16* (18), 4543-52.

6. Rachez, C.; Suldan, Z.; Ward, J.; Chang, C. P.; Burakov, D.; Erdjument-Bromage, H.; Tempst, P.; Freedman, L. P., A novel protein complex that interacts with the vitamin D3 receptor in a ligand-dependent manner and enhances VDR transactivation in a cell-free system. *Genes Dev* **1998,** *12* (12), 1787-800.

7. Rachez, C.; Lemon, B. D.; Suldan, Z.; Bromleigh, V.; Gamble, M.; Naar, A. M.; Erdjument-Bromage, H.; Tempst, P.; Freedman, L. P., Ligand-dependent transcription activation by nuclear receptors requires the DRIP complex. *Nature* **1999,** *398* (6730), 824-8.

8. vom Baur, E.; Zechel, C.; Heery, D.; Heine, M. J.; Garnier, J. M.; Vivat, V.; Le Douarin, B.; Gronemeyer, H.; Chambon, P.; Losson, R., Differential ligand-dependent interactions between the AF-2 activating domain of nuclear receptors and the putative transcriptional intermediary factors mSUG1 and TIF1. *EMBO J* **1996,** *15* (1), 110-24.

9. Le Douarin, B.; Nielsen, A. L.; Garnier, J. M.; Ichinose, H.; Jeanmougin, F.; Losson, R.; Chambon, P., A possible involvement of TIF1 alpha and TIF1 beta in the epigenetic control of transcription by nuclear receptors. *EMBO J* **1996,** *15* (23), 6701-15.

10. Tagami, T.; Lutz, W. H.; Kumar, R.; Jameson, J. L., The interaction of the vitamin D receptor with nuclear receptor corepressors and coactivators. *Biochem Biophys Res Commun* **1998,** *253* (2), 358-63.

11. (a) Guenther, M. G.; Lane, W. S.; Fischle, W.; Verdin, E.; Lazar, M. A.; Shiekhattar, R., A core SMRT corepressor complex containing HDAC3 and TBL1, a WD40-repeat protein linked to deafness. *Genes Dev* **2000,** *14* (9), 1048-57; (b) Huang, E. Y.; Zhang, J.; Miska, E. A.; Guenther, M. G.; Kouzarides, T.; Lazar, M. A., Nuclear receptor corepressors partner with class II histone deacetylases in a Sin3-independent repression pathway. *Genes Dev* **2000,** *14* (1), 45-54; (c) Wei, L. N.; Hu, X.; Chandra, D.; Seto, E.; Farooqui, M., Receptor-interacting protein 140 directly recruits histone deacetylases for gene silencing. *J Biol Chem* **2000,** *275* (52), 40782-7; (d) Potter, G. B.; Beaudoin, G. M., 3rd; DeRenzo, C. L.; Zarach, J. M.; Chen, S. H.; Thompson, C. C., The hairless gene mutated in congenital hair loss disorders encodes a novel nuclear receptor corepressor. *Genes Dev* **2001,** *15* (20), 2687-701.

12. (a) MacDonald, P. N.; Haussler, C. A.; Terpening, C. M.; Galligan, M. A.; Reeder, M. C.; Whitfield, G. K.; Haussler, M. R., Baculovirus-mediated expression of the

human vitamin D receptor. Functional characterization, vitamin D response element interactions, and evidence for a receptor auxiliary factor. *J Biol Chem* **1991,** *266* (28), 18808-13; (b) Sone, T.; Ozono, K.; Pike, J. W., A 55-kilodalton accessory factor facilitates vitamin D receptor DNA binding. *Mol Endocrinol* **1991,** *5* (11), 1578-86.

13.   Ozono, K.; Liao, J.; Kerner, S. A.; Scott, R. A.; Pike, J. W., The vitamin D-responsive element in the human osteocalcin gene. Association with a nuclear proto-oncogene enhancer. *J Biol Chem* **1990,** *265* (35), 21881-8.

14.   Shaffer, P. L.; Gewirth, D. T., Structural basis of VDR-DNA interactions on direct repeat response elements. *EMBO J* **2002,** *21* (9), 2242-52.

15.   Rochel, N.; Wurtz, J. M.; Mitschler, A.; Klaholz, B.; Moras, D., The crystal structure of the nuclear receptor for vitamin D bound to its natural ligand. *Molecular cell* **2000,** *5* (1), 173-9.

16.   MacLaughlin, J. A.; Anderson, R. R.; Holick, M. F., Spectral character of sunlight modulates photosynthesis of previtamin D3 and its photoisomers in human skin. *Science* **1982,** *216* (4549), 1001-3.

17.   Blunt, J. W.; DeLuca, H. F.; Schnoes, H. K., 25-hydroxycholecalciferol. A biologically active metabolite of vitamin D3. *Biochemistry* **1968,** *7* (10), 3317-22.

18.   Fraser, D. R.; Kodicek, E., Unique biosynthesis by kidney of a biological active vitamin D metabolite. *Nature* **1970,** *228* (5273), 764-6.

19.   Haddad, J. G., Jr.; Walgate, J., 25-Hydroxyvitamin D transport in human plasma. Isolation and partial characterization of calcifidiol-binding protein. *J Biol Chem* **1976,** *251* (16), 4803-9.

20.   Lamprecht, S. A.; Lipkin, M., Chemoprevention of colon cancer by calcium, vitamin D and folate: molecular mechanisms. *Nature reviews. Cancer* **2003,** *3* (8), 601-14.

21.   Sakaki, T.; Kagawa, N.; Yamamoto, K.; Inouye, K., Metabolism of vitamin D3 by cytochromes P450. *Frontiers in bioscience : a journal and virtual library* **2005,** *10*, 119-34.

22.   David Feldman, J. W. P., John S. Adams, *Vitamin D*. 3rd ed.; Elsevier Inc.: 2011; Vol. 1.

23.   McDonnell, D. P.; Mangelsdorf, D. J.; Pike, J. W.; Haussler, M. R.; O'Malley, B. W., Molecular cloning of complementary DNA encoding the avian receptor for vitamin D. *Science* **1987,** *235* (4793), 1214-7.

24.   Teichert, A.; Arnold, L. A.; Otieno, S.; Oda, Y.; Augustinaite, I.; Geistlinger, T. R.; Kriwacki, R. W.; Guy, R. K.; Bikle, D. D., Quantification of the vitamin D receptor-coregulator interaction. *Biochemistry* **2009,** *48* (7), 1454-61.

25.   Fox, J. D.; Waugh, D. S., Maltose-binding protein as a solubility enhancer. *Methods Mol Biol* **2003,** *205*, 99-117.

26.   Riggs, P., Expression and purification of recombinant proteins by fusion to maltose-binding protein. *Molecular biotechnology* **2000,** *15* (1), 51-63.

27.   Maina, C. V.; Riggs, P. D.; Grandea, A. G., 3rd; Slatko, B. E.; Moran, L. S.; Tagliamonte, J. A.; McReynolds, L. A.; Guan, C. D., An Escherichia coli vector to express and purify foreign proteins by fusion to and separation from maltose-binding protein. *Gene* **1988,** *74* (2), 365-73.

28.   Kruger, N. J., The Bradford method for protein quantitation. *Methods Mol Biol* **1994,** *32*, 9-15.

29.   Bradford, M. M., A rapid and sensitive method for the quantitation of microgram quantities of protein utilizing the principle of protein-dye binding. *Analytical biochemistry* **1976,** *72*, 248-54.

30.   Rosenberg, I. M., *Protein Analysis and Purification Bechtop Techniques*. Birkhauser Boston ed.; 1996; p 55-76.

31.   Juntunen, K.; Rochel, N.; Moras, D.; Vihko, P., Large-scale expression and purification of the human vitamin D receptor and its ligand-binding domain for structural studies. *The Biochemical journal* **1999,** *344 Pt 2*, 297-303.

32.   Dandliker, W. B.; Hsu, M. L.; Levin, J.; Rao, B. R., Equilibrium and kinetic inhibition assays based upon fluorescence polarization. *Methods in enzymology* **1981,** *74 Pt C*, 3-28.

33.   Checovich, W. J.; Bolger, R. E.; Burke, T., Fluorescence polarization--a new tool for cell and molecular biology. *Nature* **1995,** *375* (6528), 254-6.

34.   Wowor, V. J. L. a. A. J., *Applications of Fluorescence Anistropy to the Study of Protein-DNA Interactions; Methods in Cell Biology,* . Elsevier: 2008; Vol. 84.

35.   Fumiko Kimura, M. M., Eiji Sato, Asuka Shimba, Stuart r. Huckins, and Nobuhiko Onda, Application of Fluorescence Polarization to Molecular Biology. *Analytical Sciences* **2001,** *17*.

36.   Rossi, A. M.; Taylor, C. W., Analysis of protein-ligand interactions by fluorescence polarization. *Nature protocols* **2011,** *6* (3), 365-87.

37.   Hakamata, W.; Sato, Y.; Okuda, H.; Honzawa, S.; Saito, N.; Kishimoto, S.; Yamashita, A.; Sugiura, T.; Kittaka, A.; Kurihara, M., (2S,2'R)-analogue of LG190178 is a major active isomer. *Bioorganic & medicinal chemistry letters* **2008,** *18* (1), 120-3.

38.   Perakyla, M.; Malinen, M.; Herzig, K. H.; Carlberg, C., Gene regulatory potential of nonsteroidal vitamin D receptor ligands. *Molecular endocrinology* **2005,** *19* (8), 2060-73.

39.   Pantoliano, M. W.; Petrella, E. C.; Kwasnoski, J. D.; Lobanov, V. S.; Myslik, J.; Graf, E.; Carver, T.; Asel, E.; Springer, B. A.; Lane, P.; Salemme, F. R., High-density miniaturized thermal shift assays as a general strategy for drug discovery. *Journal of biomolecular screening* **2001,** *6* (6), 429-40.

40.   Ericsson, U. B.; Hallberg, B. M.; Detitta, G. T.; Dekker, N.; Nordlund, P., Thermofluor-based high-throughput stability optimization of proteins for structural studies. *Analytical biochemistry* **2006,** *357* (2), 289-98.

41.   Phillips, K.; de la Peña, A. H., The Combined Use of the Thermofluor Assay and ThermoQ Analytical Software for the Determination of Protein Stability and Buffer Optimization as an Aid in Protein Crystallization. In *Current Protocols in Molecular Biology*, John Wiley & Sons, Inc.: 2001.

42.   Juntunen, K. Functional and Structural Characterization of Nuclear Vitamin D Receptor and Its Ligand Binding Domain. University of Oulu, OULUN YLIOPISTO, OULU, 2002.

43.   Antharavally, B. S.; Mallia, K. A.; Rosenblatt, M. M.; Salunkhe, A. M.; Rogers, J. C.; Haney, P.; Haghdoost, N., Efficient removal of detergents from proteins and peptides in a spin column format. *Analytical biochemistry* **2011,** *416* (1), 39-44.

44.   Bruylants, G.; Wouters, J.; Michaux, C., Differential scanning calorimetry in life science: thermodynamics, stability, molecular recognition and application in drug design. *Current medicinal chemistry* **2005,** *12* (17), 2011-20.

45.   John J. Correia, H. W. D., III, *Methods in Cell Biology, Biophysical Tools for Biologists: Vol. 1 In Vitro Techniques*. Elsevier: 2008; Vol. 84.

46.   O'Brien, R.; Haq, I., Applications of Biocalorimetry: Binding, Stability and Enzyme Kinetics. In *Biocalorimetry 2*, John Wiley & Sons, Ltd: 2005; pp 1-34.

47.   Freire, E., Statistical thermodynamic analysis of differential scanning calorimetry data: structural deconvolution of heat capacity function of proteins. *Methods in enzymology* **1994,** *240*, 502-30.

48.   Privalov, P. L.; Dragan, A. I., Microcalorimetry of biological macromolecules. *Biophysical chemistry* **2007,** *126* (1-3), 16-24.

49.   Privalov, G.; Kavina, V.; Freire, E.; Privalov, P. L., Precise scanning calorimeter for studying thermal properties of biological macromolecules in dilute solution. *Analytical biochemistry* **1995,** *232* (1), 79-85.

50.   Plotnikov, V. V.; Brandts, J. M.; Lin, L. N.; Brandts, J. F., A new ultrasensitive scanning calorimeter. *Analytical biochemistry* **1997,** *250* (2), 237-44.

51.   Chaudhary, P. M.; Chavan, S. R.; Shirazi, F.; Razdan, M.; Nimkar, P.; Maybhate, S. P.; Likhite, A. P.; Gonnade, R.; Hazara, B. G.; Deshpande, M. V.; Deshpande, S. R., Exploration of click reaction for the synthesis of modified nucleosides as chitin synthase inhibitors. *Bioorganic & medicinal chemistry* **2009,** *17* (6), 2433-40.

9. APPENDIX A: Fluorescence Polarization Graphs, Figures 25-35

Summary of fluorescence polarization assay with VDR-LBD protein purified under different conditions and coactivator peptide SRC2-3.
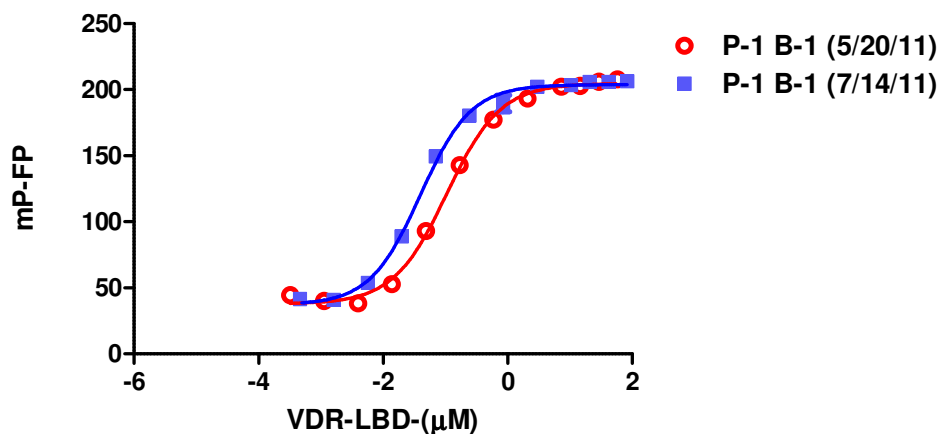
Figure-25 Fluorescence Polaziration graph for VDR-LBD Protein-1 Batch-1 purified on two different days. The sigmoidal dose-response curve suggests that the VDR-LBD protein is active. The K_d values are summarized in **table-3**.
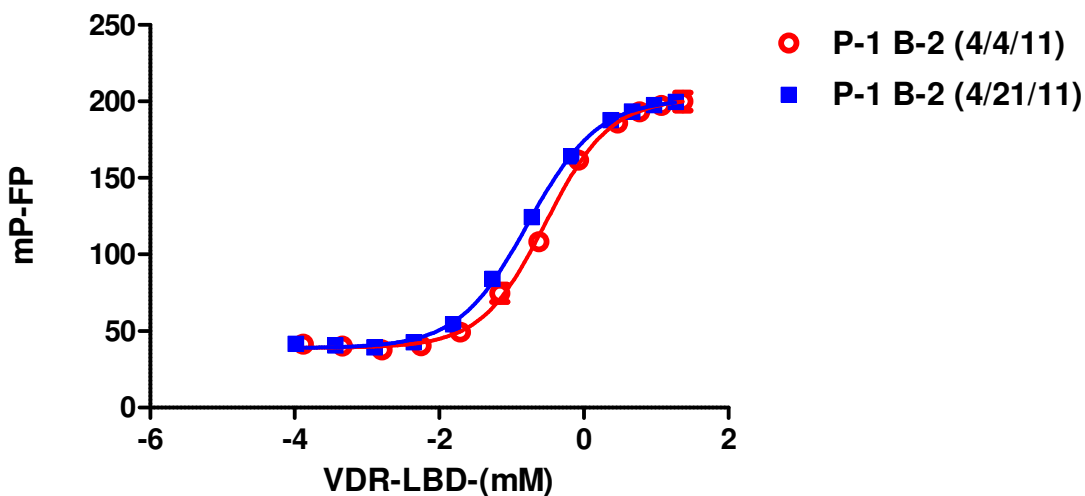
Figure-26 Fluorescence Polaziration graph for VDR-LBD Protein-1 Batch-2 purified on two different days. The sigmoidal dose-response curve suggests that the VDR-LBD protein is active. The K_d values are summarized in **table-3**.
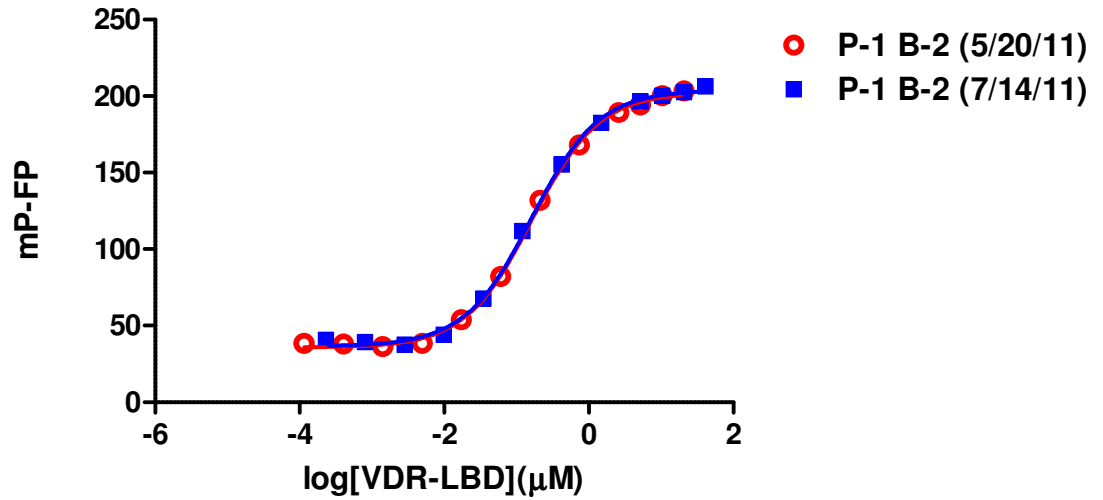
Figure-27 Fluorescence Polaziration graph for VDR-LBD Protein-1 Batch-2 purified on two different days. The sigmoidal dose-response curve suggests that the VDR-LBD protein is active. The K_d values are summarized in **table-3**.
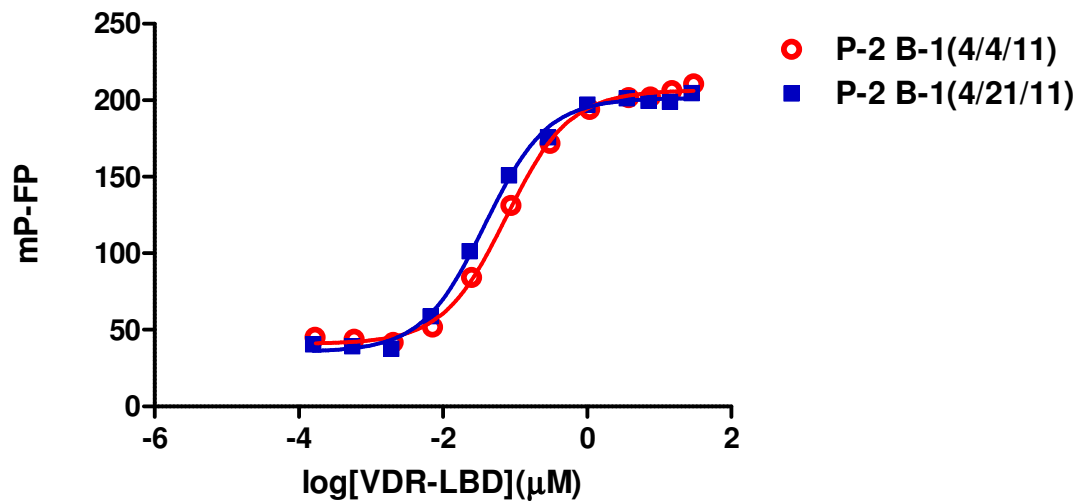
Figure-28 Fluorescence Polaziration graph for VDR-LBD Protein-2 Batch-1 purified on two different days. The sigmoidal dose-response curve suggests that the VDR-LBD protein is active. The K_d values are summarized in **table-3**.
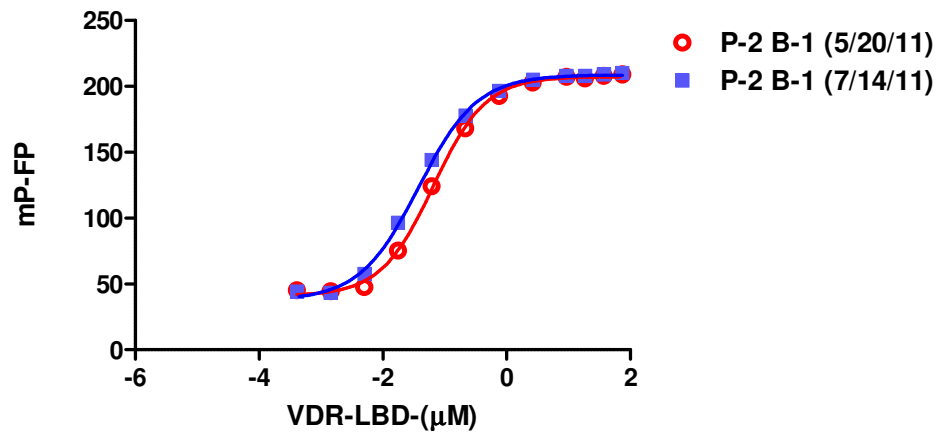
Figure-29 Fluorescence Polaziration graph for VDR-LBD Protein-2 Batch-1 purified on two different days. The sigmoidal dose-response curve suggests that the VDR-LBD protein is active. The K_d values are summarized in **table-3**.
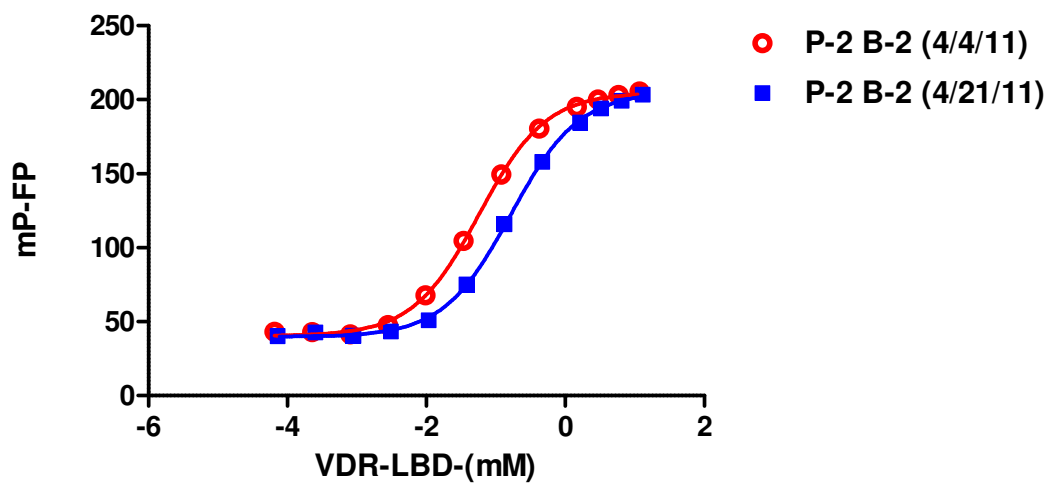
Figure-30 Fluorescence Polaziration graph for VDR-LBD Protein-2 Batch-1 purified on two different days. The sigmoidal dose-response curve suggests that the VDR-LBD protein is active. The K_d values are summarized in **table-3**.
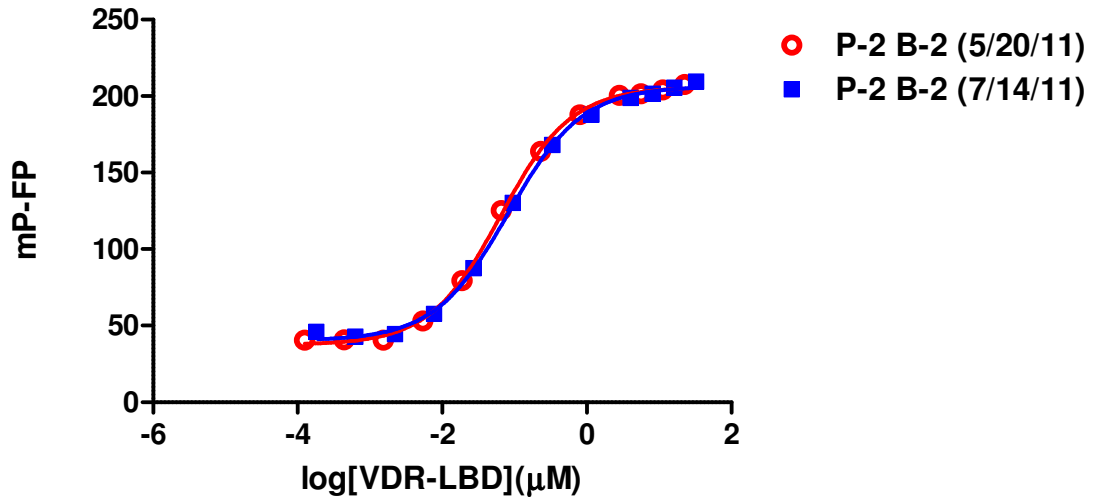
Figure-31 Fluorescence Polaziration graph for VDR-LBD Protein-2 Batch-1 purified on two different days. The sigmoidal dose-response curve suggests that the VDR-LBD protein is active. The K_d values are summarized in **table-3**.
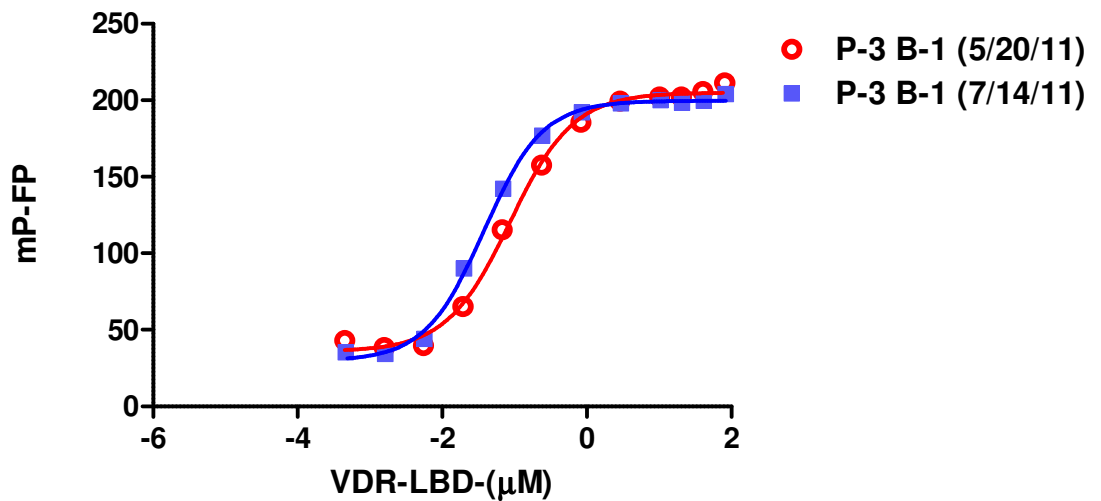
Figure-32 Fluorescence Polaziration graph for VDR-LBD Protein-2 Batch-1 purified on two different days. The sigmoidal dose-response curve suggests that the VDR-LBD protein is active. The K_d values are summarized in **table-3**.
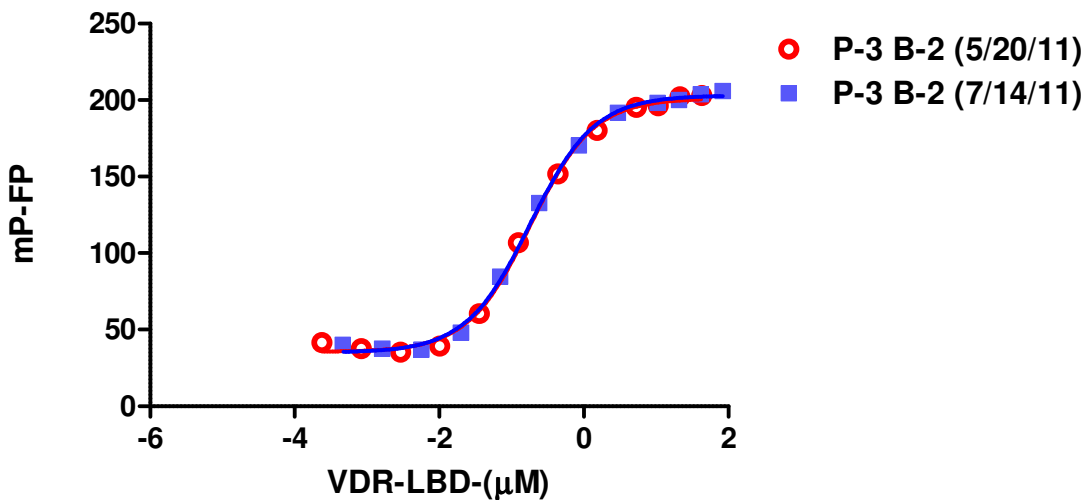
Figure-33 Fluorescence Polaziration graph for VDR-LBD Protein-2 Batch-1 purified on two different days. The sigmoidal dose-response curve suggests that the VDR-LBD protein is active. The K_d values are summarized in **table-3**.
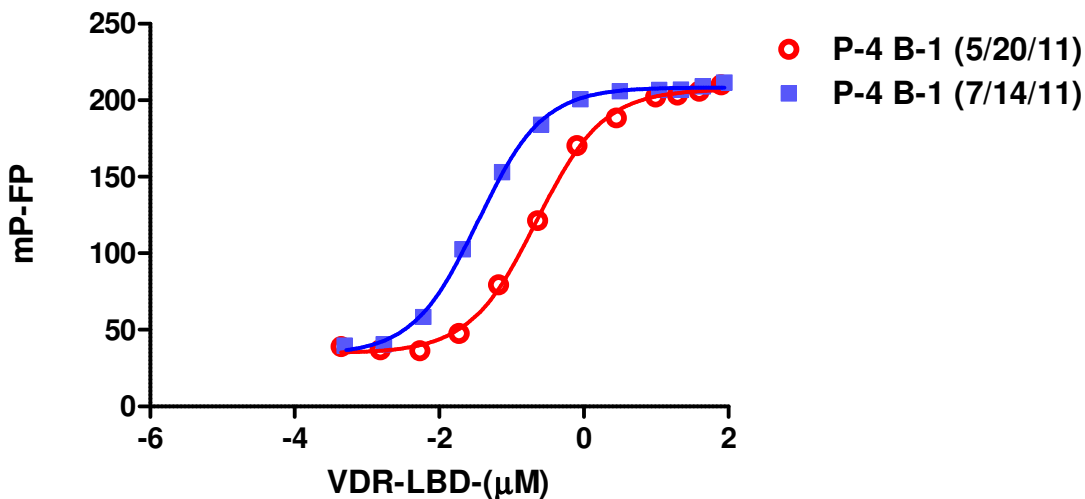
Figure-34 Fluorescence Polaziration graph for VDR-LBD Protein-2 Batch-1 purified on two different days. The sigmoidal dose-response curve suggests that the VDR-LBD protein is active. The K_d values are summarized in **table-3**.
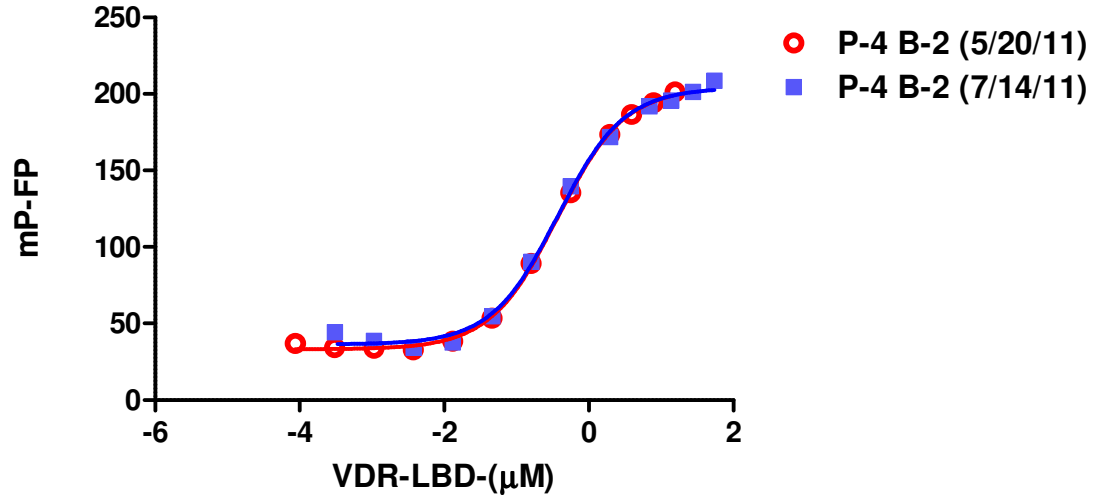
Figure-35 Fluorescence Polaziration graph for VDR-LBD Protein-2 Batch-1 purified on two different days. The sigmoidal dose-response curve suggests that the VDR-LBD protein is active. The K_d values are summarized in **table-3**.

10.APPENDIX B: Publications